Optimization of the Potency and Pharmacokinetic Properties of a Macrocyclic Ghrelin Receptor Agonist (Part I): Development of Ulimorelin (TZP-101) from Hit to Clinic

ARTICLE *in* JOURNAL OF MEDICINAL CHEMISTRY · NOVEMBER 2011

Impact Factor: 5.45 · DOI: 10.1021/jm2007062 · Source: PubMed

22 AUTHORS, INCLUDING:

Eric Marsault
Université de Sherbrooke

René Gagnon
Université de Sherbrooke

Shridhar Bhat
Johns Hopkins Medicine

Mark Peterson
TRANZYME, INC.

Journal of Medicinal Chemistry

Article

pubs.acs.org/jmc

Optimization of the Potency and Pharmacokinetic Properties of a Macrocyclic Ghrelin Receptor Agonist (Part I): Development of Ulimorelin (TZP-101) from Hit to Clinic†

Hamid R. Hoveyda,* Eric Marsault, René Gagnon, Axel P. Mathieu, Martin Vézina, Annick Landry, Zhigang Wang, Kamel Benakli, Sylvie Beaubien, Carl Saint-Louis, Martin Brassard, Jean-François Pinault, Luc Ouellet, Shridhar Bhat, Mahesh Ramaseshan, Xiaowen Peng, Laurence Foucher, Sophie Beauchemin, Patrick Bhérer, Daniel F. Veber, Mark L. Peterson, and Graeme L. Fraser

Tranzyme Pharma Inc., 3001, 12e Avenue Nord, Sherbrooke, QC J1H 5N4, Canada

Supporting Information

ABSTRACT: High-throughput screening of Tranzyme Pharma's proprietary macrocycle library using the aequorin Ca^{2+}-bioluminescence assay against the human ghrelin receptor (GRLN) led to the discovery of novel agonists against this G-protein coupled receptor. Early hits such as **1** (K_i = 86 nM, EC_{50} = 134 nM) though potent in vitro displayed poor pharmacokinetic properties that required optimization. While such macrocycles are not fully rule-of-five compliant, principally due to their molecular weight and clogP, optimization of their pharmacokinetic properties proved feasible largely through conformational rigidification. Extensive SAR led to the identification of **2** (K_i = 16 nM, EC_{50} = 29 nM), also known as ulimorelin or TZP-101, which has progressed to phase III human clinical trials for the treatment of postoperative ileus. X-ray structure and detailed NMR studies indicated a rigid peptidomimetic portion in **2** that is best defined as a nonideal type-I′ β-turn. Compound **2** is 24% orally bioavailable in both rats and monkeys. Despite its potency, in vitro and in gastric emptying studies, **2** did not induce growth hormone (GH) release in rats, thus demarcating the GH versus GI pharmacology of GRLN.

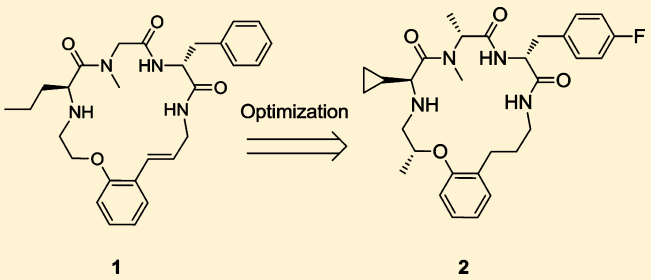

INTRODUCTION

An important unresolved issue in medicinal chemistry is the discovery of viable lead candidates. Natural ligands[1] to biological receptors, such as GPCRs, include high molecular weight structures, such as peptides, wherein optimal interactions presumably require a larger surface area. Such endogenous ligands are generally dismissed as viable leads if not due to their synthetic complexity, then because of their nonconformity to the rule-of-five,[2] inter alia due to molecular weight concerns. Yet nature provides myriad examples of structures that while in flagrant violation of the rule-of-five display good PK properties and are indeed orally bioavailable drugs. For instance, cyclosporine, a macrocyclic undecapeptide, and rapamycin, a macrocyclic polyketide, are cases in point.[3] In addition to their macrocyclic framework, such natural products have strong conformational biases due to strategically placed additional conformational constraint elements, e.g. *N*-methylation of amide bonds or stereospecific methylations on the cyclic scaffold. It is also recognized that cyclic structures tend to display lower than expected polar surface area owing to the ability to hide H-bond donors and acceptors inside the core of the molecule.[4] Much is known about the principles underlying the aforementioned conformational designs.[5,6] Moreover, analysis of factors that influence oral bioavailability in a large compound database by Veber and co-workers led to the realization that elements of the rule-of-five are surrogates for rotatable bond count that is in turn a measure of molecular flexibility.[7] The work described herein was guided by conformational design as a principal tenet, both in terms of conception of the initial screening library as well as the subsequent optimization of the generated lead structures for improved potency and PK properties.

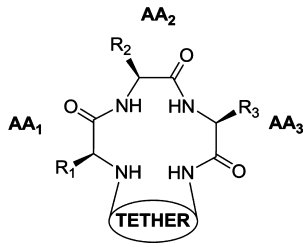

Figure 1. General structure of the Tranzyme Pharma macrocycles (depicted stereochemistry for illustration).

Received: June 2, 2011

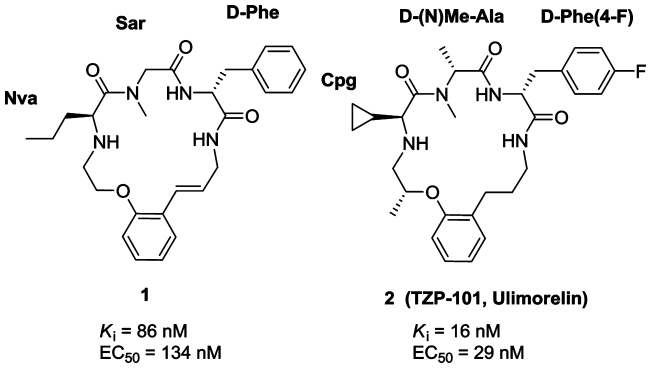

Figure 2. Structures of the initial GRLN agonist lead (**1**) and the clinical candidate, ulimorelin (**2**).

The proprietary library developed at Tranzyme Pharma[8] offers an approach to conformationally restricted macrocyclic peptidomimetic compounds (Figure 1).[9] This library has proven notably successful in generating agonist and antagonist lead candidates for ligands at GPCRs such as the MOT-R[10] and GRLN receptors. Both of these peptidic GPCR ligands are stimulants of GI motility. Ghrelin is an octanoylated 28-mer peptide that was discovered in 1999 as the endogenous ligand of GRLN[11] (previously termed the human growth hormone secretagogue receptor, hGHS-R1a).[12] The latter belongs to a GPCR receptor superfamily, each of which is activated by a peptide bearing an obligatory positively charged amine residue, i.e. the so-called GPCR-PA(+) family.[13] In contrast to the early recognition of its GH-releasing properties,[14] the gastroprokinetic effects of ghrelin peptide have only been appreciated recently.[15] In the clinic, ghrelin has been shown to accelerate gastric emptying (GE) in healthy volunteers[16] and in patients with diabetic or idiopathic gastroparesis.[17] In this paper, we document the viability of macrocycle **1** (Figure 2) as a lead GRLN agonist for the development of macrocycle **2** (ulimorelin, TZP-101), a clinical candidate currently in phase III human trials.[18] On the basis of the phase II clinical trial data,[19] it appears that the gastroprokinetic property of ulimorelin helps restore GI function in postoperative ileus (POI) and in related conditions such as acute diabetic gastroparesis. It is noteworthy that **2** displays more profound effects on GI activity than on GH release in rats[20] and humans[18b] unlike other full agonists of GRLN.[21,22] In the context of this unique property of **2**, it is pertinent to note the observations by Holst and co-workers who have shown that ligand-specific bias and/or agonist−allosteric signaling can be relevant for peptide and nonpeptide GRLN agonists.[23] As such, ulimorelin (**2**) serves to demarcate the in vivo pharmacology of GRLN in terms of GH vis-à-vis GI prokinetic effects and thus should additionally serve as a valuable tool for a better understanding of the workings of this physiologically important GPCR.

Compound **1** (Figure 2) was one of two potential lead structures detected in our HTS campaign and was designated for further development. In addition to being sufficiently potent

Scheme 1. Solution Synthesis of Compound 2 (Method C)[a]

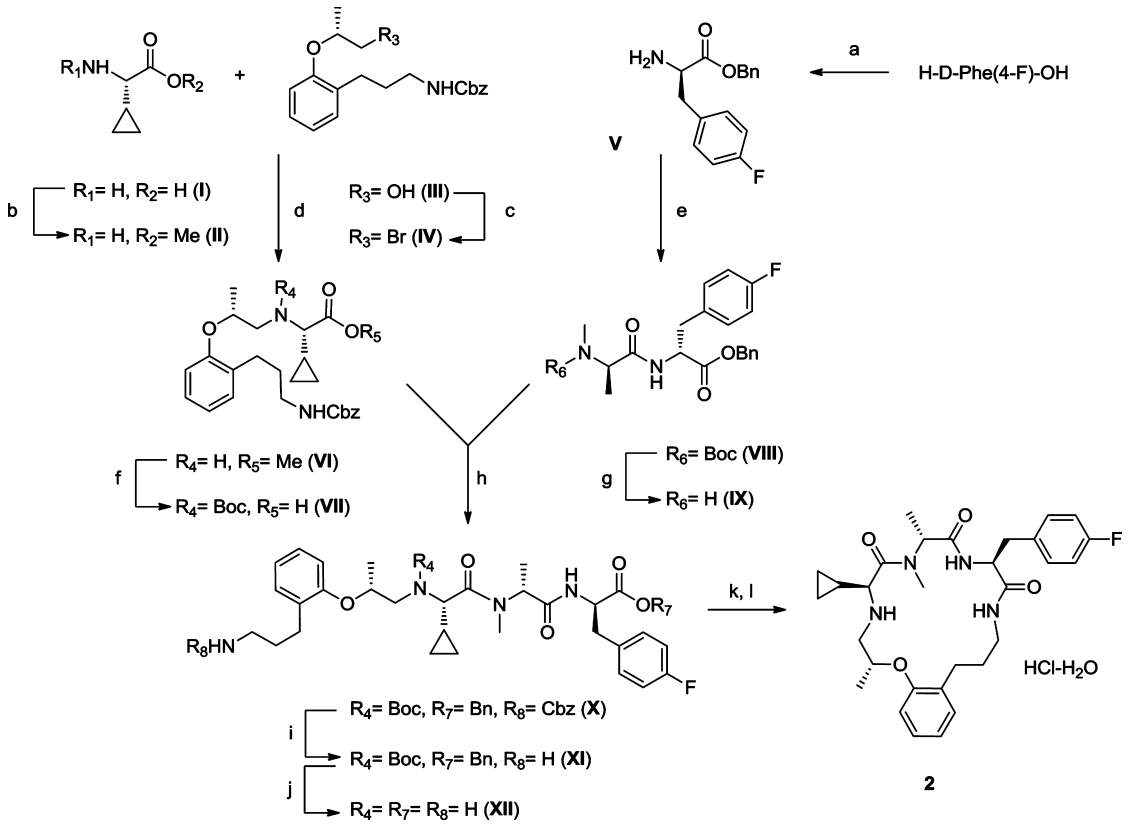

[a]Reagents and conditions: (a) (i) BnOH, TsOH, (ii) Na_2CO_3; (b) (i) AcCl, MeOH, (ii) Na_2CO_3; (c) NBS, PPh_3; (d) Na_2CO_3, KI, 100 °C; (e) Boc-(D)NMeAla-OH, EDCI, (6-Cl)HOBt, $iPrEt_2N$; (f) (i) Boc_2O, Na_2CO_3, (ii) LiOH; (g) HCl, dioxane; (h) HATU, $iPrEt_2N$; (i) 10% Pd/C, H_2; (j) HCl, dioxane; (k) DEPBT, $iPrEt_2N$; (l) (i) EtOH, HCl, (ii) EtOH/H_2O recrystallization, (iii) MEK/H_2O recrystallization.

Table 1. Tripeptide (AA_{1-3}) SAR in the Macrocyclic GRLN Lead Agonists

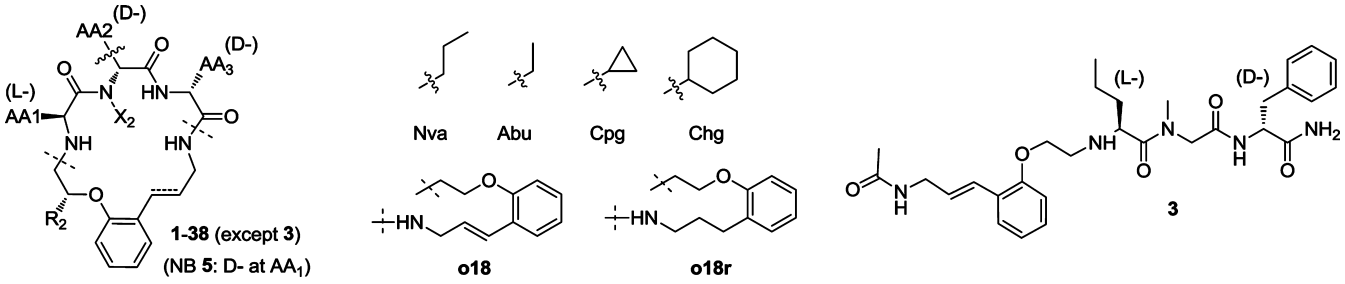

compd	AA_1	AA_2	AA_3	X_2	R_2	tether	method	K_i (nM)	EC_{50} (nM)
1	Nva	Gly	D-Phe	Me	H	o18	A	86	134
2	Cpg	D-Ala	D-Phe(4-F)	Me	Me	o18r	A, C	16	29
3	Nva	Gly	D-Phe	Me	H	o18-Ac[a]	A	>10000	ND[b]
4	Nva	Gly	D-Phe	Me	H	o18r	A	68	83
5	D-Nva	Gly	D-Phe	Me	H	o18r	A	1200	ND
6	Nva	Gly	Phe	Me	H	o18r	A	380	ND
7	Ser	Gly	D-Phe	Me	H	o18r	A	>10000	ND
8	Lys	Gly	D-Phe	Me	H	o18r	A	1100	ND
9	Glu	Gly	D-Phe	Me	H	o18r	A	>10000	ND
10	Phe	Gly	D-Phe	Me	H	o18r	A	670	ND
11	Nva	Gly	D-Nle	Me	H	o18r	A	400	ND
12	Nva	Gly	D-Tyr	Me	H	o18r	A	120	39
13	Nva	Gly	D-Ser	Me	H	o18r	A	>10000	ND
14	Nva	Gly	D-Glu	Me	H	o18r	A	>10000	ND
15	Nva	Gly	D-Orn	Me	H	o18r	A	>10000	ND
16	Leu	D-Ala	D-Phe	Me	H	o18r	A	25	ND
17	Ile	D-Ala	D-Phe	Me	H	o18r	A	6.4	ND
18	Cpg	D-Ala	D-Phe	Me	H	o18r	A	4.4	23
19	Nva	D-Ala	D-Phe	Me	H	o18r	A	16	40
20	Nva	Ala	D-Phe	Me	H	o18r	A	580	ND
21	Nva	D-Ala	D-Phe	H	H	o18r	A	500	ND
22	Ile	D-Abu	D-Phe	H	Me	o18r	A	35	ND
23	Ile	D-Val	D-Phe	H	Me	o18r	A	380	ND
24	Ile	D-Ala	D-Hfe	Me	H	o18r	A	43	ND
25	Ile	D-Ala	D-Phe(4-Cl)	Me	H	o18r	A	0.35	20
26	Nva	D-Ala	D-Phe(4-F)	Me	Me	o18r	A	34	ND
27	Val	D-Ala	D-Phe(4-F)	Me	Me	o18r	A	104	ND
28	Ile	D-Ala	D-Phe(4-F)	Me	Me	o18r	A	32	ND
29	Cpg	D-Ala	D-Phe(4-Cl)	Me	Me	o18r	A	15	18
30	Cpg	D-Ala	D-Phe	Me	Me	o18r	A	34	ND
31	Cpg	D-Ala	D-Phe(2-F)	Me	H	o18r	A	6.2	ND
32	Cpg	D-Ala	D-Phe(3-F)	Me	H	o18r	A	21	ND
33	Cpg	D-Ala	D-Phe(4-F)	Me	H	o18r	A	7.3	ND
34	Cpg	D-Ala	D-Phe(4-CF_3)	Me	H	o18r	A	7.0	11
35	Cpg	D-Ala	D-Phe(4-Me)	Me	H	o18r	A	5.0	8.2
36	Cpg	D-Ala	D-Phe(3*S*-Me,4-F)	Me	Me	o18r	A, C	4.8	51
37	Cpg	D-Ala	D-Phe(3*R*-Me,4-F)	Me	Me	o18r	A, C	75	100
38	Chg	D-Ala	D-Phe(4-F)	Me	Me	o18r	A	0.38	49

[a]o18-Ac refers to the acetylated o18 tether; cf. structure **3** in the graphic illustration for this table. [b]ND = not determined.

both in GRLN radioligand binding assay (K_i = 86 nM) and a full agonist in the aequorin assay (EC_{50} = 134 nM), analogue **1** exhibited >100-fold selectivity against MOT-R, the most germane receptor to GRLN.[24] Furthermore, **1** displayed no cytotoxicity up to 100 μM (HepG2 assay) and demonstrated tractable structure–activity relationships (SAR) as discussed below. Nonetheless, this early lead structure and related analogues displayed poor PK in rats that required optimization. We undertook a two-pronged approach for further lead optimization of **1**. This consisted of both a systematic side-chain modification of the tripeptide moiety (cf. AA_{1-3} in Figure 1), aimed principally at improving receptor binding, as well as introducing steric interactions in the tether portion of the structure that might restrict the conformation (to the bioactive form), thereby limiting access to clearance mechanisms that would in turn diminish oral bioavailability and shorten in vivo half-life. A combination of these approaches proved necessary for the discovery and development of the preclinical candidate, ulimorelin (**2**, Figure 2), as detailed below.

Chemistry. The general chemistry for the synthesis of the analogues described herein relied both on solid-phase and solution synthetic methodologies. The method of preparation for each analogue discussed is specified in the table of results (Tables 1−3) based on the nomenclature defined below. The two solid-phase parallel synthetic approaches used herein, so-called methods A and B, for the synthesis of the macrocyclic targets have been detailed elsewhere.[8,10] Briefly, method A[25] employed a thioester-activated linker for cyclative-release macrolactamization,[26] whereas method B invoked Ru-catalyzed ring-closing metathesis in a cyclative-release fashion. Minor modifications to these published methods were required due to the presence of sterically encumbered *N*-methyl amino acids[27] at the AA_2 position. These modifications entailed (i) the use of the more reactive HATU[28] (instead of HBTU) as the activating agent, and (ii) two successive treatments each with 2.5 equiv excess of the AA_1 reagent to form the amide bond at the AA_1−AA_2 juncture (instead of a single coupling with 5 equiv excess of the AA_1 building block previously described). Irrespective of the methodology employed, the crude products were purified by silica gel column chromatography and/or mass spectrometry triggered reverse-phase HPLC.[29] Building blocks, whether amino acids or tethers (Figure 1) that were not available commercially, were either prepared through literature procedures or were otherwise synthesized as described in the Supporting Information.

In the later stages of the lead optimization program, solution-phase synthetic approaches were investigated given the scale-up demands for clinical studies. Shown in Scheme 1 is the convergent macrolactamization approach that was ultimately employed, with minor modifications,[30] for the kilogram cGMP scale-up of the clinical candidate, compound **2**. In this synthetic approach, the acyclic precursor (**X**, Scheme 1) was obtained in protected form by amide coupling of the AA_2−AA_3 dipeptide benzyl ester fragment (**IX**) with the primary amine protected form of AA_1−tether fragment (**VII**). The Boc-protected AA_2−AA_3 dipeptide fragment (**VIII**) was prepared by using EDCI and 6-Cl-HOBt as the amide coupling reagents (step e, Scheme 1). The AA_1−tether fragment was prepared through direct alkylation by reacting H-Cpg-OMe (**II**) with the bromoalkyl form of tether (**IV**).[31] For the macrolactamization step, DEPBT[32] was eventually selected as the coupling agent of choice based on the overall isolated yields and diastereomeric purity criteria. The Scheme 1 procedure furnished the final macrocyclic product (**2**), with less than 0.1% diastereomeric impurity on any of the stereogenic centers. Also noteworthy is the high macrocyclization yields (>80%), typically obtained without recourse to the high dilution conditions (≤0.03M) usually required for such reactions, ca. 0.05 M reagent concentration was often used. These observations tend to suggest the preorganized nature of the acyclic precursors (**XI** in Scheme 1). Following the DEPBT-mediated macrocyclization step,[33] **2** in free base form was converted to its corresponding HCl salt and recrystallized, as a purification step, to thereby obtain the product in the ethanolate HCl salt form. The latter salt, after a subsequent recrystallization in MEK/H_2O, furnished the preferred hydrated HCl salt form that eventually served as the API for the clinical studies.

RESULTS AND DISCUSSION

In the foregoing discussions, emphasis is placed on receptor affinity (i.e., K_i values) for the elucidation of SAR, rather than on functional assays wherein SAR can be more difficult to discern based on potential bias due to the choice of the signal transduction pathway, as well as constitutive GRLN signaling and the potential for agonist−allosteric activation.[23]

As a first step in the optimization of compound **1** (Figure 2), the indispensability of the macrocyclic ring structure was established through lack of GRLN potency displayed by the analogous acyclic congener (cf. **3** in Table 1). Next, the styrenyl double bond in the so-called o18 tether (see Table 1 illustrations) was reduced to furnish compound **4** (cf. Table 1). When **4** was seen to result in no significant loss of binding potency, the olefin-reduced tether (o18r) was chosen as the basis for further study to circumvent the potential metabolic liability of the styrenyl moiety. Additional tether SAR is outlined further below (cf. Tables 2−3).

Tripeptide SAR. Summarized in Table 1 is a representative list of compounds that highlight the SAR of the tripeptide portion of the lead structure (cf. AA_{1-3} in Figure 1). Stereochemical SAR was established through the use of D- and L-amino acids. For each of the three amino acid positions, a clear stereochemical SAR trend was discernible.

At the AA_1 position, an ∼18-fold preference was observed for L- rather than D-amino acids bearing aliphatic residues (cf. **4** vs **5**, Table 1). Analogues with polar (**7**), ionizable (**8**, **9**), or aromatic side-chains (**10**) were poorly tolerated. Branching at the β-position of an amino acid can have a significant impact on the local backbone conformation of a peptide. Ramachandran recognized this effect along with a more significant impact of the presence of a γ-atom on side-chain conformation in his now classic work.[34] In the early generation leads, β-branched amino acid side-chains at AA_1 provided the most potent analogues.[36b] Thus **17**, AA_1 = Ile and **18**, AA_1 = Cpg were in the 4−6 nM potency range clearly superior to **19**, AA_1 = Nva (K_i = 16 nM) and **16** AA_1 = Leu (K_i = 25 nM). In the advanced leads, the following potency order emerged: Cpg (**2**) > Ile (**28**) ≈ Nva (**26**) ≫ Val (**27**). The latter trend though less precipitous, given the near parity of potency between Ile (**28**) and Nva (**26**), still indicated Cpg (**2**) as nearly 2-fold more potent vs Ile (**28**) and 6.5-fold more so vs Val (**27**, K_i = 104 nM). Overall, early in the project, a decision was made to retain Cpg as the favored AA_1 amino acid, despite its appreciably higher cost vs Ile, not merely because of the 2-fold potency difference, but based on the following reasons: (i) the cyclopropyl group in Cpg is smaller and more conformationally restricted than *sec*-butyl in Ile, and (ii) the a priori considerations that cyclopropyl is regarded to be more metabolically stable than other alkyl groups, as it is much more stable to hydrogen abstraction.[35]

The stereochemical SAR at the AA_2 site was equally remarkable as that at AA_1. Thus a ∼36-fold preference was noted for D- rather than L- amino acids (cf. **19** vs **20**). Moreover, it was also clear that *N*-methylation at the AA_2 site is also a significant (∼31-fold) contributor to potency, evinced through comparing the *N*-Me congener **19** (K_i = 16 nM) to the related des-Me congener **21** (K_i = 500 nM). The significant potency effect of combined D-configuration and *N*-methylation at AA_2 is likely through conformational impact as turn inducers (cf. Structural Studies section below).[36] Extension of the *N*-Me group whether through straight chain or branched homologation was counterproductive (cf. **17** vs **22**−**23**). Hence, despite an extensive survey of various amino acids, AA_2 = D-NMe-Ala was maintained as the amino acid at that position for the remainder of the project.

Several substitutions at AA_3 proved successful in improving potency and were explored further. The stereochemical

Table 2. Tether SAR: Impact of Tether Linker Moieties

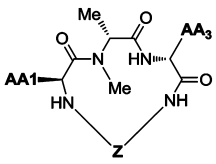

39-40

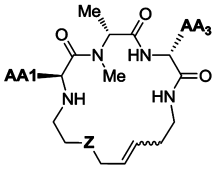

41

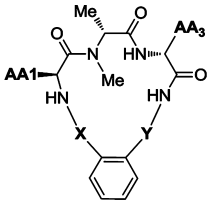

17,33,42-45

compd	AA_1	AA_2	X	Y	Z	ring	method	K_i (nM)	EC_{50} (nM)
39	Ile	D-Phe			$(CH_2)_7$	17	B	>10000	ND
40	Ile	D-Phe			$(CH_2)_8$	18	B	1500	ND
41	Ile	D-Phe			CH_2	18	B	160, 170[a]	310, 330[a]
42	Ile	D-Phe	$(CH_2)_3$	$(CH_2)_2$		17	A	400	ND
43	Ile	D-Phe	$(CH_2)_2O$[b]	$(CH_2)_2$		17	A	210	530
44	Ile	D-Phe	$(CH_2)_3$	$(CH_2)_3$		18	B	81	ND
45	Ile	D-Phe	$(CH_2)_3$	$(CH_2)_4$		19	B	78	360
33	Cpg	D-Phe(4-F)	$(CH_2)_2O$	$(CH_2)_3$		18	A	7.3	ND
17	Ile	D-Phe	$(CH_2)_2O$	$(CH_2)_3$		18	A	6.4	ND

[a]Attributable to *E* or *Z* olefins in the tether moiety, which was separated by HPLC. [b]Counterclockwise from the AA_1 amine nitrogen to the tether amide nitrogen, when read left to right.

Table 3. Tether SAR: Tether Backbone Substitutions (Unspecified Substitutents Are Hydrogen)

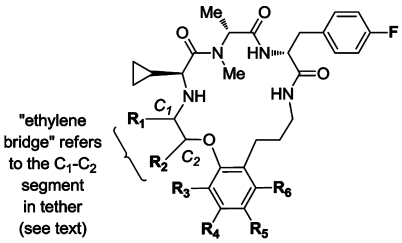

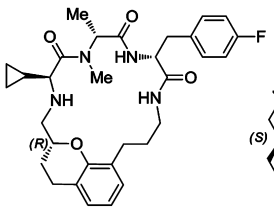

49

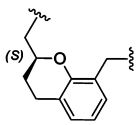

50

compd	tether substitution(s)	method	K_i (nM)	EC_{50} (nM)
2	R_2 = (*R*)-Me	A	16	29
33	none	A	7.3	ND
46	R_1 = (*R*/*S*)-Me	A	9.0	760
47	R_2 = (*S*)-Me	A	56	26
48	R_2 = *gem*-dimethyl	A	12	partial agonist[a]
49	(see illustration above)	A[b]	0.90	85
50	(see illustration above)	A[b]	19	ND
51	R_4 = F	A	2.6	27
52	R_5 = F	A	58	ND
53	R_2 = (*R*)-Me, R_4 = F	A	61	ND

[a]~40% agonist response at 3 μM test concentration. [b]A solution-phase variant synthesis of method A was also used (see Supporting Information for details).

preference at this position was for D-amino acids (cf. **4** vs **6**), although less pronounced (5.5-fold) than that at AA_1 and AA_2 positions. In addition, a penchant for hydrophobic (aromatic or aliphatic) side-chain moieties (e.g., **4**, **11**, **12**) over those containing polar or ionizable groups (**13**−**15**) was abundantly clear. Homologation of the benzyl side-chain in D-Phe resulted in ~7-fold diminished potency (**24** vs **17**). Improved potency and ligand lipophilicity efficiency (LLE)[37] proved markedly feasible through phenyl ring substitutions; thus D-Phe(4-Cl) analogue **25** (LLE = 3.0) proved ~18-fold more potent than the analogous nonchlorinated congener **17** (LLE = 2.5). While *ortho* and *para* aryl substitution patterns appeared particularly favored (cf. **31**−**33**), no electronic preference was discernible as both electron-withdrawing (CF_3 in **34**, LLE = 1.6, or F in **33**, LLE = 2.4) *and* electron-donating substituents (CH_3 in **35**, LLE = 2.2) proved of comparable potency with K_i values in the 5−7 nM range. These improvements are likely to be the consequence of a favorable direct receptor interaction rather than conformational effects. The LLE trends continued to support the choice of *para* fluoro-substituted AA_3 in the advanced lead structures as well and served as a basis for its selection going forward.[38] The role of stereospecific methyl substitution on the benzylic AA_3 side-chain to restrict the so-called χ-space[39] was also explored (cf. **36**−**37** vs **2**). Interestingly, a ~3-fold improvement in potency was obtained with the *erythro*-isomer (**36** vs **2**) whereas the *threo*-isomer showed a ~5-fold deterioration in potency (**37** vs **2**). Despite this, analogue **36** was not further developed because the synthetic complexity outweighed the moderate potency gains.

Tether SAR. The tether component of the macrocyclic ghrelin agonists herein (cf. Figure 1) proved a very effective means of controlling both bioactivity and PK properties. In

terms of the ring size, an 18-membered ring proved to offer the best potency (cf. **44**−**45**, Table 2); with 17-membered rings in related analogues, significant loss of potency was observed (cf. **39** vs **40**). Also noteworthy was the observation that an olefinic tether forming an 18-membered ring devoid of any aryl component was about 10-fold *more* potent than the analogous saturated olefin tether (**41** vs **40**), possibly reflective of a conformational constraint effect due to the double bond. Moreover, it was observed that a phenyl ring serves as a bioisostere for the olefin moiety in the foregoing tethers (cf. **44** vs **41**). Finally, replacing the tether phenyl ring in **44** with a phenoxy ring (i.e., **17**) resulted in a 10-fold gain in potency together with a relative LLE gain of 1.8 log units.[40] It was further noted that the phenoxy-containing tether is superior in terms of GRLN-to-MOT-R selectivity[24] (>1:1500) vis-à-vis the olefinic tether (≤1:30).[41] Overall, these considerations led us to retain the phenoxy ring tether structure, such as in **17**, for further lead optimization.

The term "ethylene bridge" is used for brevity herein to refer to the ethylene tether segment situated between the AA_1 secondary amine and the tether phenoxy oxygen (see illustration in Table 3). This so-called ethylene bridge was regarded as potentially both electron-rich and conformationally flexible and was therefore selected as a potential target for PK improvement in these macrocycles. Accordingly, we employed a two-pronged approach of conformational rigidification of the ethylene bridge (e.g., through C_1/C_2 methyl substitutions) and modulation of the electronic properties in the phenoxy ring in the tether (e.g., through R_4/R_5 fluorophenyl substitutions). (Results related to conformational rigidification elsewhere in the tether backbone will be described in the sequel to this report.) A selection of such tether variations together with their impact on the pharmacodynamic (PD) and/or PK profiles is summarized in Tables 3−4).

Methyl substitution at the C_1 carbon in the ethylene bridge (**46**) retained the binding potency but worsened the functional efficacy (EC_{50} = 760 nM, cf. Table 3). In contrast, stereospecific methyl substitutions at the adjacent C_2 carbon atom resulted in both good binding potency and functional efficacy. Thus the R_2 = (*R*)-Me tether (**2**) proved to be ∼3.5 more potent than its (*S*)-Me epimer (**47**). In contrast, the related *gem*-dimethyl substituted analogue (**48**) proved to be a partial agonist despite displaying good binding potency (cf. Table 3). Further conformationally restricted variants of analogues **2** and **47** were achieved by incorporating chiral benzopyran rings that join the C_2 carbon in the ethylene bridge with the phenoxy ring (cf. **49**−**50**). Mirroring the trends observed with the Me-substituted congeners (**2** vs **47**), once again the (*R*)-benzopyran analogue (**49**) proved to be more potent than its (*S*)-epimer (**50**), with the proviso that in these latter more conformationally restricted analogues, the potency gap had widened with **49** (K_i = 0.90 nM) being ∼21-fold more potent than its epimer **50** (K_i = 19 nM).

The phenoxy ring tether displayed clear SAR in terms of ring substitution patterns. For instance, fluorophenyl substitution at the R_4 tether position (**51**, K_i = 2.6 nM, Table 3) resulted in ∼2-fold improved binding potency (vs **33**, K_i = 7.3 nM, Table 1). Shifting the fluoro-substitution from R_4 to R_5 (**51** vs **52**), i.e. from the *para* benzylic to the *para* phenoxy position, degraded the potency by ∼22-fold. As further elucidated in the Structural Studies section below, the latter SAR trend correlates with the observation of an intramolecular H-bond, discernible in both solution and solid-state, between the phenoxy oxygen and the protonated secondary amine at the AA_1 position that is likely a further contributor to the conformational rigidity in these analogues. Thus, substitution of an electron withdrawing group *para* to the phenoxy oxygen would lower the basicity of oxygen and thereby weaken the said H-bond. Finally, an analogue that contained both R_2 = (*R*)-Me and R_4 = F tether features (**53**, K_i = 61 nM) displayed worse potency than either of its progenitors (**51**, K_i = 2.6 nM, or **2**, K_i = 22 nM). The impact of such tether structural variants on the PK SAR is described below.

PK and ADME Profile Analyses. Factors that relate physicochemical properties of a molecule to absorption play a crucial role in the pharmacokinetics of orally administered drugs.[2,42] A commonly upheld paradigm in this context is the so-called Lipinski's rule-of-five.[2] While POI treatment, as the primary clinical application intended, requires a parenteral route of administration, it was nonetheless necessary to establish that the foregoing macrocycles are amenable to optimization toward low systemic clearance rates (CL) and good oral bioavailability to support further chronic clinical applications in related GI disorders requiring a prokinetic agent.

Shown in Table 4 are the PK data in rats for a selection of analogues in this project. Male Sprague−Dawley rats were administered compounds either as an IV bolus at 2 mg/kg in physiological saline with 9% 2-hydroxypropyl-β-cyclodextrin and/or PO (gavage) at 8 mg/kg in physiological saline. Two tether modifications in particular proved of great impact on the PK profile: (i) stereospecific substitution at the R_2 tether position (see Table 3 illustration), for example R_2 = (*R*)-Me (**2**) or (*R*)-benzopyran (**49**), and (ii) fluorophenyl substitution at the R_4 tether position (**51**). Indeed, when both tether features were combined (e.g., **53**, Table 4), additional improvement of CL and plasma half-life ($T_{1/2}$) was obtained albeit at the expense of a deteriorated potency. Thus, analogue **53** was cleared from systemic circulation in rats at a rate of 9 mL/min/kg with a $T_{1/2}$ of 66 min and a volume of distribution 50% higher than that of total body water. Furthermore, a clear PK SAR was evident in terms of the configuration of the Me substitution at the R_2 tether position in the ethylene bridge. Thus, with R_2 = (*R*)-Me in **2** relatively low CL of 24 mL/min/kg was observed with $T_{1/2}$ = 50 min, whereas the corresponding R_2 = (*S*)-Me epimer (**47**) cleared at significantly higher rates (CL = 64 mL/min/kg) with a much shorter $T_{1/2}$ of 22 min. Indeed, the improved PK profile with R_2 = (*R*)-Me tether substitution extended to the fused-ring (*R*)-benzopyran congener (**49**) that cleared at a further reduced rate of 13 mL/min/kg, with $T_{1/2}$ = 59 min and a volume of distribution nearly twice that of total body water. Therefore, the additional conformational rigidification from **2** to **49** was rewarding not only in terms of ∼18-fold improved binding potency (cf. Table 3) but also with respect to ∼2-fold improved CL. Nonetheless, the additional synthetic complexity in **49** vs **2** on the one hand, and the diminished agonist potency (EC_{50}, Table 3) and lower volume of distribution (cf. Table 4) on the other, favored the selection of analogue **2** (ulimorelin) for clinical development as a parenteral treatment of POI.

It should be emphasized that the tether design was a necessary though insufficient condition to attain an improved PK profile of reduced CL and longer $T_{1/2}$. In fact a so-called "PK cooperative effect" was observed in **2** wherein *both* stereospecific R_2 = (*R*)-Me tether (see Table 3 illustration) *and* the cyclopropyl AA_1 side-chain proved critical to its improved PK profile. Comparison of the PK profile of analogues **2** vs **26**−

Table 4. PK Profile and GE Data (IV Administration) in Rats

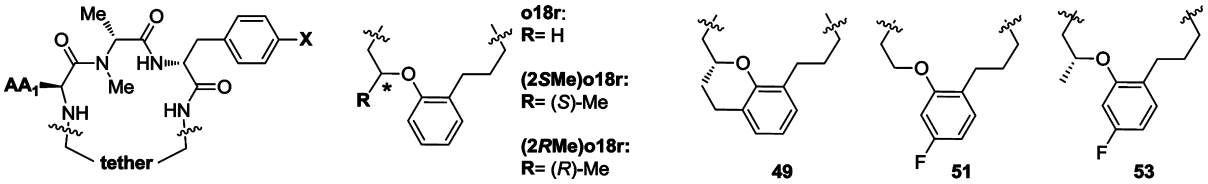

compd	AA_1	X	tether	PO, 8 mg/kg C_{max} (μM)	PO, 8 mg/kg $AUC_{0-\infty}$ (μM·min)	IV, 2 mg/kg $T_{1/2}$ (min)	IV, 2 mg/kg V_{dss} (L/kg)	IV, 2 mg/kg CL (mL/min/kg)	%F	IV GE EC_{50} (mg/kg)
	ghrelin peptide			ND	ND	ND	ND	ND	ND	0.04
2	Cpg	F	(2*R*Me)o18r	0.39	82.0	50	1.7	24	24	0.91
25	Ile	Cl	o18r	0.06	3.51	33	3.2	67	3	0.39
26	Nva	F	(2*R*Me)o18r	ND	ND	29	1.7	41	ND	ND
27	Val	F	(2*R*Me)o18r	ND	ND	34	2.0	40	ND	ND
28	Ile	F	(2*R*Me)o18r	ND	ND	44	2.5	40	ND	ND
29	Cpg	Cl	(2*R*Me)o18r	0.67	73.8	41	1.4	24	22	0.84
30	Cpg	H	(2*R*Me)o18r	ND	ND	32	1.3	25	ND	ND
33	Cpg	F	o18r	ND	ND	14	1.4	72	ND	ND
38	Chg	F	(2*R*Me)o18r	ND	ND	74	4.7	43	ND	ND
47	Cpg	F	(2*S*Me)o18r	ND	ND	22	2.1	64	ND	ND
49	Cpg	F	*see figure*	ND	ND	59	1.1	13	ND	ND
51	Cpg	F	*see figure*	0.90	99.9	44	1.8	28	36	1.20
53	Cpg	F	*see figure*	0.75	125	66	0.9	9	15	1.38

Table 5. Physiochemical, Efflux Properties, and Micrsomoal Stability Profile for 2, 25, and 51

compd	MW (g/mol)	clogP	H-bond donors	H-bond acceptors	Caco-2 flux (nm/s)[a] s-to-m	Caco-2 flux (nm/s)[a] m-to-s	RLM %compd[c]	HLM[b] $T_{1/2}$ (min)
2	538.6	5.3	3	5	140	150	68	19
25	557.1	6.4	3	5	150	140	86	5
51	542.6	5.1	3	5	125	198	54	41

[a]For reference, propranolol, a high permeability compound displays Caco-2 flux values of ca. 350 nm/s. [b]For reference, human liver microsome (HLM) $T_{1/2}$ value for propranolol was 59 min. [c]Refers to %compd metabolized after 15 min.

28 (Table 4) abundantly highlights this cooperative effect in terms of the role of the AA_1 cyclopropyl side-chain.[43] Thus, **2** displayed ~2-fold improved clearance rate (CL = 24 mL/min/kg) and was 24% orally bioavailable in rats versus related structures (**26**−**28**) that differed *only* in terms of the nature of the AA_1 side chains (Nva, Val, Ile) and showing significantly higher CL of ≥40 mL/min/kg.[44] On the other hand, comparison of analogues **2** and **33** underscores the importance of the R_2 = (*R*)-Me tether to achieving improved PK. Thus, **33** with AA_1 = Cpg but with an *unsubstituted* ethylene bridge displayed essentially flow-limited clearance (CL = 72 mL/min/kg) with a concomitantly short $T_{1/2}$ of 14 min. A potential rationale for this cooperative effect that is evidently crucial in obtaining improved PK profile is provided at the conclusion of the Structural Studies section.

In contrast to the aforesaid key role of the AA_1 side chain in modulating PK, variations in the AA_3 side chain were largely uneventful. For example, analogue **29** (CL = 24 mL/min/kg, %*F* = 22) with a *para* chlorophenyl AA_3 side-chain exhibited a similar CL and oral bioavailability in rats when compared to its fluoro congener **2** (CL = 24 mL/min/kg, %*F* = 24). In fact, even the unsubstituted AA_3 phenyl ring (**30**) showed similar clearance rates to **2** and **29** (cf. Table 4). Therefore, the AA_3 phenyl ring metabolism is likely not a major elimination pathway in such macrocycles. This was later confirmed based on a more detailed metabolite study on analogue **2**.

It has been recognized that oral availability of compounds may be, at least in part, a function of metabolism by cytochrome P-450 (CYP) enzymes and/or transporter efflux mechanisms mediated by P-glycoproteins (Pgp). As shown in Table 5, the serosal-to-mucosal and mucosal-to-serosal in vitro permeabilities in rat distal colon (Caco-2 assay) show that neither AA_1 = Cpg nor R_2 = (*R*)-Me tether features are required for attaining good membrane permeability given that **25** (AA_1 = Ile and R_2 = H) showed comparable in vitro permeability to **2** (AA_1 = Cpg and R_2 = (*R*)-Me). In fact, neither **2** nor **25**, both of which displayed moderate permeability, appear to be Pgp substrates given the near parity of flux rates in both directions. However, in vitro, analogue **2** displayed a greater rat (RLM) and human hepatic liver microsomal (HLM) metabolic stability as compared to **25** (cf. Table 5). This suggests that the improved CL and oral bioavailability in **2** vs **25** is possibly the result of improved first-pass hepatic and/or intestinal metabolism, perhaps mediated by CYP enzymes. In contrast, with the R_4 = F tether design (**51**, Table 4) 60% higher permeability was detected in the m-to-s against s-to-m direction, possibly suggesting a moderate Pgp active transport uptake effect. The higher PO C_{max} for **51** at 0.90 μM (vs 0.39 μM for **2**, Table 4) also tends to substantiate the in vitro permeability outlook. In addition, the R_4 = F tether design in **51** further improved RLM and HLM stability even against **2**. Moreover, compound **51** displayed a 36% oral bioavailability in rats. Overall, these results tend to suggest that

Table 6. PK Profile in Monkeys and Human CYP Profile for 2 and 51

	PO, 8 mg/kg		IV, 2 mg/kg				CYP IC_{50} (μM)				
compd	C_{max} (μM)	$AUC_{0-\infty}$ (μM·min)	$T_{1/2}$ (min)	V_{dss} (L/kg)	CL (mL/min/kg)	%*F*	3A4	2D6	2C9	2C19	1A2
2	1.4	75.4	23	0.23	8.8	24	2.4	84	66	>100	>100
51	0.09	10.3	29	0.66	20	7	1.2	31	>100	>100	>100

improved rat PK profile in R_4 = F tether designs (e.g., **51**, **53**) may be due to both improved first-pass clearance and enhanced absorption assisted by Pgp active transport.

Following a 30 min. IV infusion at a target dose level of 6 mg/kg in Sprague–Dawley rats, ^{14}C-labeled **2** was efficiently excreted in the feces unchanged with a recovery of 95% of the administered dose.[45] These results are consistent with hepatobiliary elimination and would suggest that **2** is subject to liver first-pass effect after PO dosing. It is also noteworthy that **2** displayed a reasonably high unbound fraction in rat plasma (f_u = 13%).[46]

Shown in Table 6 are PK data in monkeys for analogues **2** and **51** that displayed good overall PD and PK profiles. Adult male cynomolgus monkeys (*Macaca fascicularis*) were administered compounds either as an IV bolus at 0.5 mg/kg in physiological saline with 9% 2-hydroxypropyl-β-cyclodextrin, and/or PO (gavage) at 1.5 mg/kg in physiological saline. Whereas **2** displayed identical oral bioavailability in monkeys and rats (%*F* = 24, cf. Tables 4 and 6), the bioavailability of compound **51** in monkeys (%*F* = 7, Table 6) was nearly 5-fold lower than what was observed in rat (%*F* = 36, Table 4). Parallel CL trends followed for the two compounds; thus, in monkeys, **2** (CL = 8.8 mL/min/kg) was cleared 2.3 times more slowly than **51** (CL = 20 mL/min/kg), representing a greater disparity versus the same trends observed in rats wherein both analogues cleared at similar rates (CL = 24 and 28 mL/min/kg for **2** and **51**, respectively).[47] In addition, the overall CYP profile for **2** appeared somewhat superior to **51** (Table 6) even though both analogues displayed suboptimal CYP 3A4 profiles that are nonetheless acceptable for the acute POI treatment intended. These considerations together with the GE in vivo efficacy results (vide infra) confirmed **2** as the clinical candidate of choice.

In Vitro and in Vivo Pharmacology. In each successive hit-to-lead optimization library, every analogue was initially screened in competitive radioligand binding assays performed on isolated membranes expressing GRLN, using ^{125}I-His-9 octanoylated ghrelin peptide as radioligand.[48] The most potent compounds were in turn screened in the Ca^{2+}-bioluminescence aequorin functional assay conducted in HEK-293 cells expressing human GRLN.[49] The data from the radioligand binding and functional assays (cf. Tables 1–3) are derived from duplicate samples where the maximum tolerated interassay variability was ±10%. Compound **2** was tested repeatedly, as a reference, in binding (N = 4) and aequorin functional assays (N = 3) with intra-assay data (mean ± SD) of K_i = 18 ± 1 nM and EC_{50} = 27 ± 2 nM, respectively. All compounds reported are full agonists of GRLN except analogue **48** (cf. Table 3); full agonism is defined as a maximal response >70% of that for the endogenous ligand, i.e. octanoylated human ghrelin peptide.[12]

A similar order of potency was observed for the analogues tested in both radioligand binding and cell-based functional assays, although comparison of the latter results revealed a nonmonotonic shift between the receptor affinity and efficacy of these macrocyclic GRLN agonists compared to ghrelin peptide.[11] Otherwise stated, while ghrelin is ∼400-fold more potent than **2** in binding assays, a mere ∼20-fold difference separates them in the functional assay. This indicates high intrinsic agonist efficiency in these macrocyclic agonists. Additionally, the aequorin functional assay was predictive for the efficacy of compounds in the rat GE assay (IV dosing): once again, only ∼20-fold difference was detected in terms of GI prokinetic effects of **2** vis-à-vis ghrelin peptide. The prokinetic GE response is immediate to IV dosing and accordingly even structures with high CL such as ghrelin peptide and **25** proved effective in rat GE studies (IV route). However, neither ghrelin nor **25** would be orally efficacious due to high first-pass clearance. That aside, even with IV administration, neither **25** nor ghrelin peptide would provide the sustained activity likely required for treatment of such ailments as POI and are thus unsuitable on that basis as therapeutics of choice.

PK profiling in rats highlighted certain analogues, such as **2** and **51** (cf. Table 4), that demonstrated improved oral bioavailability consistent with their lower CL and superior RLM stability (cf. Table 5). In agreement with PK data in rats, oral efficacy for compounds **2** and **51** was confirmed in the rat GE assays as well (cf. Figure 3). However as stated above, PK

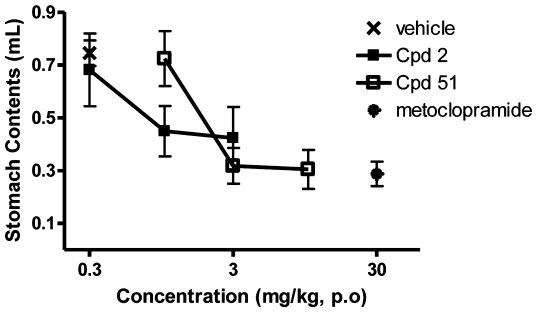

Figure 3. Rat GE Data (PO) for compounds **2** and **51**.

profiling in monkeys revealed **2** as superior to **51** in terms of CL and %*F* (cf. Table 6). As adumbrated above, the superior potency of analogue **2** in the rat GE assays (IV and PO) served as a further basis for the selection of this compound for clinical development. Importantly, **2** also demonstrated an excellent preliminary safety profile devoid of binding Na^+ and K^+ channels (up to 10 μM), no significant inhibition of hERG in patch-clamp assays (up to 30 μM), as well as excellent off-target receptor selectivity (CEREP ExpresSProfile screen) and no genotoxicity concerns based on a clean profile in the AMES test (up to 5000 μg/plate).

Structural Studies. *Single Crystal X-ray Studies.* The solid-state structure of compound **2** was determined in various solvates and salt forms using single crystal X-ray crystallography (Figure 4a). Overlay of the five X-ray structures clearly demonstrates that whereas the tripeptide backbone conformations are nearly superimposable, the tether moiety is conformationally fluxional. Thus, heavy atom root-mean-square deviation (rmsd) of 0.5 Å vs 2.5 Å was obtained when comparing the tripeptide against the tether segment in **2** (Figure 4a). In

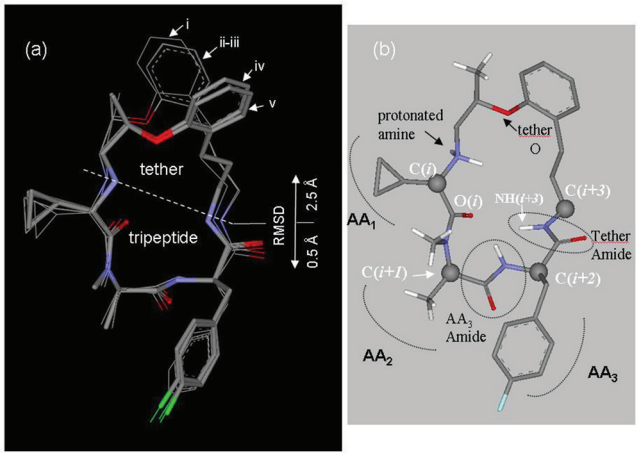

Figure 4. (a) Superposition of the five X-ray crystal structures of **2**: (i) hemisuccinate−EtOH; (ii−iii) HCl·H_2O and HCl·2H_2O (overlap nearly perfectly), (iv) HCl·EtOH, and (v) HCl·1·6MeCN. (Counter-ions, solvent molecules and hydrogen atoms are omitted for clarity.) (b) Definition of the structural terminologies used throughout this section.

addition, the following observations were made upon detailed analysis of bond distance and torsion angle (ϕ, ψ, ω) data (see Supporting Information):[50] (i) in all five single crystal X-ray structures, the Cα(i)−Cα(i + 3) distances (cf. Figure 4b) are less than 7 Å, indicative of a β-turn,[51,52] and (ii) the torsion angles in the tripeptide segment revealed a type I′ β-turn.[53] Essentially the same conclusions were also reached through analysis of the solution NMR structure discussed below. Interestingly, a key similarity between the X-ray and NMR structures was the presence of an *intra*molecular H-bond chelate ring that was observed between the tether phenoxy oxygen and an ammonium hydrogen at AA_1 (Figure 4b), based on distances that are significantly shorter than the sum of the van der Waals radii.[54] We in fact postulate that this intramolecular H-bond is likely imparting further conformational rigidity on the macrocyclic framework that in turn may impact the improved PK profile in **2** as further elaborated below.

Solution NMR Studies. Solution conformation analysis of **2** was performed by a combination of NMR spectroscopy and molecular modeling as detailed in the Supporting Information (section 4.II). Only a single conformational family was consistent with all the experimental NMR constraints, with the average structure representing the consensus solution conformation (cf. Figure 5). Several additional NMR data supported the solution conformational homogeneity in **2**: (i) the presence of discrete ^{1}H NMR signals for *each* of the tether backbone geminal protons, even those not adjacent to a stereocenter;[55] (ii) the presence of a large $^3J_{NH\text{-}H\alpha}$ (≥8 Hz) vicinal coupling for the D-Phe(4-F) moiety at the (i + 2) corner residue, i.e. the AA_3 position[56] (cf. Figure 4b);[57] (iii) the disparity between the $^3J_{NH\text{-}C\alpha}$ values for the (i + 2), or AA_3 amide, and that in the adjacent (i + 3) residue, the so-called tether amide (cf. Figure 4b), i.e. $^3J_{NH\text{-}H\alpha} \geq 8$ Hz vs ∼5 Hz, respectively;[58] (iv) a clear differentiation of the temperature gradients for the exchangeable AA_3 and tether amide protons.[59] These observations together with torsion angle analyses (cf. Supporting Information, section 4.I) are collectively consistent with a conformationally rigid tripeptide moiety in **2** that can be defined as a (nonideal) closed type I′ β-turn.

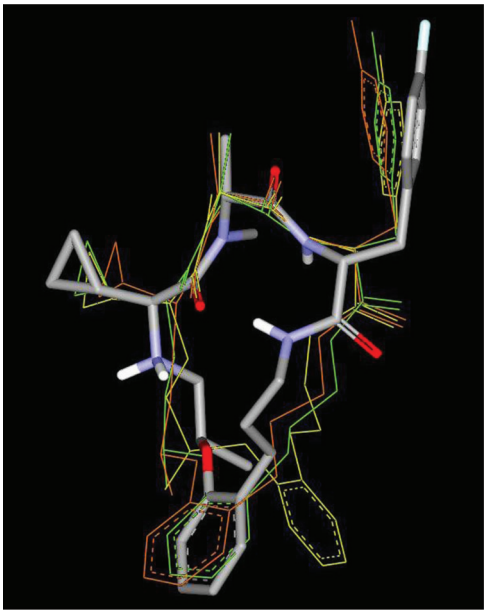

Figure 5. Superposition of the solution NMR consensus structure (in bold stick presentation with standard atom color schemes) and representative solid-state conformations (hemisuccinate−EtOH in red, HCl·H_2O in green, and HCl·EtOH form in yellow line representation).

The solution NMR average structure resembles the solid-state X-ray structures overall (cf. Figure 5) as stated previously. It is noteworthy to recall that the intramolecular H-bond between the tether phenoxy oxygen and the AA_1 protonated secondary amine was observed in *both* the solid-state *and* solution structures of **2**. Additionally, in the NMR structure, the ammonium hydrogen also appears H-bonded to the C═O at AA_1 (NH···O═C, 2.4 Å), thus producing two tandem H-bond chelate rings that may further contribute to the conformational rigidity in **2**.

On the PK Cooperative Effect and the Interplay between the Cyclopropyl Side Chain at AA_1 and the R_2 = (*R*)-Me Substitution in Tether. As previously stated, achieving improved PK in **2** required *both* AA_1 = Cpg *and* R_2= (*R*)-Me substitution in the tether (see Table 3 illustrations). Thus, analogues **26**−**28** and **38** (cf. Table 4), all of which contained R_2= (*R*)-Me tether substitution but differed in the nature of branched AA_1 side-chain, did not display improved PK profile in rats. Clearly these results tend to discredit the hypothesis that improved PK is achieved through metabolic blocking in R_2 = (*R*)-Me tether analogues. If the latter hypothesis were true, *every* analogue with the R_2 = (*R*)-Me tether ought to have displayed reduced CL, which was manifestly not the case. Conversely, AA_1 = Cpg alone or together with (*S*)-Me tether substitution did not result in analogues with diminished CL (cf. **33** and **49**, Table 4). The rule-of-five is unlikely to furnish additional insights here either. Therefore, we wish to reconsider in this context the potential role of the intramolecular H-bond detected both in solid-state and in solution (vide supra) between the protonated secondary amine at AA_1 and the tether oxygen in **2**.

Comparison of the Hammett σ_p and Hansch π values indicate that the cyclopropyl ring, while significantly less lipophilic, is nearly as electron-donating as the cyclohexyl ring.[60] On the one hand, the strong electron donor group effect would enhance the basicity of the secondary amine at AA_1,

thereby strengthening the said intramolecular H-bond. This is reflected in the measured pK_a values for both analogues with Cpg at AA_1 (**18** and **2**, cf. Table 1, pK_a = 6.72 ± 0.08 and 7.17 ± 0.04, respectively) in which the amine basicity is enhanced by ≥0.3 log units versus the congener with an *n*-Pr side chain (**19**, cf. Table 1, pK_a = 6.45 ± 0.08).[61] On the other hand, the relatively low lipophilicity of the cyclopropyl side-chain could impact hepatic metabolism rates as well as the solubility profile vis-à-vis other alkyl side-chains such as cyclohexyl. Furthermore, in step with the lipophilicity trends, a noticeably improved aqueous solubility was detected with AA_1 = Cpg analogues such as **2**, with the solubility values in the 1−8 mg/mL range (at ca. pH 5). Related structures with AA_1 = Nva (**26**) or Ile (**28**) showed significantly lower aqueous solubility (0.1−0.5 mg/mL range), with AA_1 = Chg analogue (**38**) very poorly soluble (≤0.01 mg/mL) under similar conditions.

Thus, the strong electron donicity of the AA_1 cyclopropyl side-chain may serve to bolster conformational rigidity in **2** by strengthening the aforesaid intramolecular H-bond within the macrocyclic core with minimal additional impact on the overall lipophilicity. Moreover, the R_2 = (*R*)-Me tether substitution and the AA_1 cyclopropyl side-chain appear to be suitably juxtaposed on opposite faces of the macrocyclic framework to provide hydrophobic shielding of the intramolecular H-bond from both sides of the molecule, thus protecting it from disruption by encroaching water molecules.[62] *As a possible basis for the observed PK cooperative effect in* **2**, *we propose that the AA_1 cyclopropyl side-chain and the R_2 = (R)-Me group are exerting electronic and steric shielding effects, respectively, to thus stabilize the aforesaid intramolecular H-bond that in turn confers additional rigidity to the macrocyclic structure.*

■ CONCLUSION

A macrocyclic GRLN agonist lead from the Tranzyme Pharma's proprietary macrocycle library proved amenable to optimization culminating in a clinical candidate with favorable potency and PK properties. This result was achieved despite initial poor PK properties seen in the early HTS hits that showed poor adherence to the rule-of-five in terms of molecular weight and clogP properties (cf. Table 5). The initial hit **1** has apparently a quite low rotatable bond count (*n*Rot = 4). However, as pointed out by Veber et al., the definition of *n*Rot as having no rotatable bonds in any ring structure is incorrect for larger rings.[7] In fact, analysis of the NMR data of **2** revealed conformational flexibility in the tether region of this macrocycle. Nature employs methyl substituents as local conformational constraint elements to improve biological properties, as elegantly exemplified in such natural products as polyketides.[6] Indeed, methyl substituents are particularly advantageous as they introduce conformational rigidification without adding to the rotatable bond count.[63] We have used this approach extensively here to progress from poor to favorable PK properties. Thus, optimizing the initial HTS hit **1** to arrive at the clinical lead candidate **2** was achieved through stereospecific methyl substitution at the AA_2 position, stereospecific methyl substitution adjacent to the phenolic oxygen of the tether, and through introduction of an AA_1 cyclopropyl side-chain. Compound **2**, now known as ulimorelin, developed following this strategy has proven to possess sufficiently favorable PK properties to warrant clinical evaluation for acute treatment of GI disorders such as POI and is currently in phase III human clinical trials. In Part II of this report, we will disclose further applications of the principles used herein to additionally improve oral bioavailability and CYP profiles that culminated in a second clinical candidate (TZP-102), for the oral treatment of chronic GI motility diseases that has progressed into phase IIb human clinical trials for diabetic gastroparesis.

■ EXPERIMENTAL SECTION

Method for GE Studies. Experiments were conducted on overnight-fasted male Wistar rats (200 ± 20 g; *N* = 5 per data point). Rats were given methylcellulose (2%) containing phenol red (0.05%) administered orally at 2 mL/animal and sacrificed 15 min later. Stomach contents were measured at sacrifice by colorimetric analysis (560 nm) for determination of phenol red remaining. For IV dosing experiments, test substances (vehicle: 9% 2-hydroxypropyl-*β*-cyclodextrin) were administered coincident with the methylcellulose meal. In all cases, compounds were tested at three concentrations (0.08, 0.3, 1.25 mg/kg) and IC_{50} values were determined by linear regression analysis. For PO dosing experiments, test substances (vehicle: 0.9% saline) were administered 30 min prior to the methylcellulose meal. The prokinetic agent metoclopramide was tested as a positive control at a maximally efficacious concentration in all experiments (IV dose 10 mg/kg; PO dose 30 mg/kg).

PK Analyses. Experiments were conducted on male Sprague−Dawley rats (250 ± 20 g; *N* = 3) with analogue **2** administered by IV bolus at 2 mg/kg in physiological saline with 9% 2-hydroxypropyl-*β*-cyclodextrin and/or PO (gavage) at 8 mg/kg in physiological saline. Each compound was likewise tested in a single experiment comprised of 3 rats. Clearance was used to evaluate interassay variability of no greater than ±18% of the mean reported value.

Similarly, analogue **2** was tested in male cynomolgus monkeys (4 ± 0.5 kg; *N* = 2 by IV bolus at 0.5 mg/kg) in physiological saline with 9% 2-hydroxypropyl-*β*-cyclodextrin and/or PO (gavage) at 1.5 mg/kg in physiological saline. In each species, over the 6 h test period, blood samples (0.25 mL) were collected at 12 time points into centrifuge tubes containing K_3EDTA and plasma samples were then immediately isolated by centrifugation and stored at −20 °C prior to analysis. Plasma concentrations of analogue **2** were determined by LCMS/MS and data were analyzed by noncompartmental methods using WinNonlin Pro (Pharsight Corp., Mountain View, CA). Analogue **51** was tested similarly.

Solution NMR Conformation Studies. Full description of methods as well as all data related to NMR structural studies on compound **2** is provided in the Supporting Information (section 4.II, pp. S37−S55).

Single Crystal X-ray Crystallography. Full description of methods as well as all data related to X-ray structural studies on compound **2** is provided in the Supporting Information (section 4.III, pp. S56−S111). Mercury 1.5.2 software (Cambridge Crystallographic Data Centre) was used for visualization and data analysis herein.

Chemical Synthesis: General Considerations. The solid-phase synthesis procedures have been disclosed in detail in previous publications.[8,10] Solution synthesis of compound **2** as per Scheme 1 is detailed below. Unprotected amino acids as well as Boc- and Fmoc-protected amino acids and coupling reagents were purchased from specialized amino acid manufacturers (Novabiochem, Advanced ChemTech, Bachem, Chem-Impex, Peptech). Reagents and chemicals were generally purchased from Aldrich or VWR. Solvents for reactions were of DriSolv quality (anhydrous) as manufactured by EM Science. Flash column chromatography was performed using silica gel 60 (230−400 mesh) (EMD Chemicals, Darmstadt, Germany). Analytical TLC was performed using silica gel 60 F_{254} precoated plates (0.25 mm thickness) with a fluorescent indicator from EMD Chemicals. All reactions were conducted at room temperature under N_2 atmosphere unless otherwise noted. NMR spectra were recorded on a Varian Mercury-VX instrument at ambient temperature. The residual (^{1}H) or solvent carbons (^{13}C) were used as internal standards. ^{1}H NMR data are presented using the standard abbreviations as follows: chemical shift (*δ*) in ppm (multiplicity, integration, coupling constant(s)). Abbreviations for multiplicities observed in NMR spectra: s, singlet; br s, broad singlet; d, doublet; t, triplet; q, quadruplet; p, pentuplet; m,

multiplet. LCMS analyses were performed using UV, ELSD, and CLND[29] detectors using XTerra MS C18 3.5 μm, 4.6 mm × 50 mm column, by employing "Grad_A4" method as detailed in Supporting Information (section 5a). Chiral LC was performed using Chiralcel OD-RH (4.6 mm × 150 mm, Chiral Technologies) as per the details provided in Supporting Information (section 5a). High-resolution mass spectra (HRMS) were recorded on a ZAB-1F instrument (VG model) using electron impact ionization or a Waters Synapt G1 time-of-flight instrument. HRMS data for all final macrocycles are provided in the Supporting Information (section 5). All compounds reported are of at least 95% purity according to LCMS[29] (conditions detailed in Supporting Information, section 5a).

Solution Synthesis of Compound 2 (Method C, Scheme 1). *(S)-Methyl 2-amino-2-cyclopropylacetate (II). Preparation of II as HCl Salt.* To a suspension of H-Cpg-OH **I** (20.0 g, 174 mmol, 1.0 equiv) in anhydrous MeOH (350 mL) at 0 °C was slowly added freshly distilled acetyl chloride (185 mL, 2.6 mol, 15 equiv) over 45 min. The mixture was allowed to warm to room temperature and stirred 16−18 h whereupon the reaction was deemed complete by TLC (MeOH/NH_4OH/AcOEt (10:2:88); R_f = 0.50 (ninhydrin)). The mixture was then concentrated in vacuo (15−30 mmHg) at 40−45 °C, azeotroped with toluene (3 × 100 mL), and dried under vacuum (1−2 mmHg) at room temperature for 16−18 h to obtain **II** in HCl salt form as pale-yellow solid (30.0 g, > 100% crude yield). ^{1}H NMR (CD_3OD) δ ppm 4.88 (s, 3H), 3.85 (s, 3H), 3.36−3.33 (d, 1H), 1.19−1.10 (m, 1H), 0.83−0.53 (m, 4H).

Preparation of II as Free Base. The hydrochloride salt obtained above was dissolved in aqueous Na_2CO_3 solution (1M; 275 mL, 0.272 mol, 1.5 equiv). The basic aqueous phase was saturated with NaCl and extracted with EtOAc/CH_2Cl_2 (2:1) (5 × 100 mL). The combined organic extracts were dried over $MgSO_4$, filtered, concentrated, and dried under vacuum (15−30 mmHg) at room temperature. The drying was monitored by ^{1}H NMR until only ca. 5% EtOAc was detectable. The amino ester **II** was thus obtained as yellow oil (19.1 g, 85%) and used without further purification. (NB: (i) Free amine **II** is a volatile product; thus care should be exercised when applying vacuum to dry this product. (ii) The product dimerizes to the corresponding diketopioperazine that crystallizes from a neat solution of free amine **II** left standing at room temperature. Thus, this product is best prepared shortly prior to use in the direct alkylation step and should be stored at −20 °C overnight.) ^{1}H NMR ($CDCl_3$) δ ppm 3.70 (s, 3H), 2.88−2.85 (d, 1H), 1.54 (s, 1H), 1.04−0.97 (m, 1H), 0.56−0.27 (m, 4H).

(R)-Benzyl (3-(2-((1-Bromopropan-2-yl)oxy)phenyl)propyl)-carbamate (IV). To the crude alcohol **III** (see Supporting Information, section 2b-2) (21.5 g, 62.6 mmol, 1.0 equiv) in anhydrous CH_2Cl_2 (250 mL) were added NBS (12.8 g, 72.0 mmol, 1.15 equiv) and PPh_3 (18.9 g, 72.0 mmol, 1.15 equiv). The round-bottom flask was wrapped in aluminum foil paper, and the mixture was stirred at room temperature 16−18 h, whereupon the reaction was deemed complete by TLC (EtOAc/hexanes (3:7); R_f = 0.42 (UV)). Saturated aqueous NH_4Cl solution (200 mL) was then added, and the aqueous phase was extracted with CH_2Cl_2 (2 × 150 mL). The combined organic extracts were washed with a saturated aqueous NH_4Cl solution (2 × 200 mL). The organic phase was dried over $MgSO_4$, filtered, and concentrated under vacuum (15−30 mmHg) at 40−45 °C. Purification of the residue by silica gel flash chromatography (500 g column) eluting with 0−15% gradient EtOAc/hexanes gave the title compound as a slightly yellow oil (22.2 g, 88.4%). LCMS (method Grad_A4): retention time 11.04 min; %purity (UV/ELSD/CLND), 100/100/99. [M + H]$^+$ = 406, 408 (Br isotope). ^{1}H NMR ($CDCl_3$) δ ppm 7.37−7.26 (m, 5H), 7.19−7.13 (m, 2H), 6.92−6.88 (t, 1H), 6.84−6.81 (d, 1H), 5.10 (s, 2H), 4.96 (br s, 1H), 4.62−4.56 (m, 1H), 3.58−3.45 (m, 2H), 3.22−3.16 (q, 2H), 2.69−2.64 (t, 2H), 1.83−1.78 (p, 2H), 1.45 (d, 3H). ^{13}C NMR ($CDCl_3$) δ ppm 156.66, 155.08, 136.99, 131.28, 130.77, 128.75, 128.32, 128.28, 127.49, 121.56, 113.03, 73.12, 66.76, 40.69, 36.12, 30.45, 27.48, 19.00.

(S)-2-(((R)-2-(2-(3-(((Benzyloxy)carbonyl)amino)propyl)phenoxy)-propyl)(tert-butoxycarbonyl)amino)-2-cyclopropylacetic Acid (VII). Preparation of precursor VI: In a predried round-bottom flask, bromide **IV** (47.2 g, 117 mmol, 1.0 equiv) and freshly free-based H-Cpg-OMe **II** (19.1 g, 148 mmol, 1.2 equiv) were added. Degassed anhydrous dimethyl formamide (117 mL), anhydrous Na_2CO_3 (14.8 g, 140 mmol, 1.2 equiv), and KI (19.4 g, 117 mmol, 1.0 equiv) were added and the mixture was stirred at 100 °C under a nitrogen atmosphere for 16−18 h, whereupon reaction was deemed complete by TLC (hexanes/EtOAc (1:1); R_f = 0.35 (UV)) and LCMS (Grad_A4; retention time, 6.68). The reaction mixture was then allowed to reach room temperature, and water (200 mL) was added. The aqueous phase was extracted with MTBE (3 × 100 mL). The combined organic extracts were washed with water (2 × 100 mL), brine (1 × 100 mL), dried over $MgSO_4$, filtered, and concentrated under vacuum (15−30 mmHg) at 40−45 °C. Purification of the residue by silica gel flash chromatography (1.1 kg column) eluting with gradient elution hexanes/EtOAc/CH_2Cl_2 (85/10/5 to 75/20/5 to 50/45/5) afforded the secondary amine **VI** as orange oil (43.1 g, 81%). LCMS (method Grad_A4): retention time, 6.63 min; %purity (UV/ELSD/CLND), 94/100/98. [M + H]$^+$ = 455.37. ^{1}H NMR ($CDCl_3$) δ ppm 7.31−7.22 (m, 5H), 7.07−7.03 (m, 2H), 6.80−6.74 (m, 2H), 5.48 (br s, 1H), 5.00 (s, 2H), 4.49−4.43 (m, 1H), 3.56 (s, 3H), 3.18−3.11 (m, 3H), 2.75−2.50 (m, 4H), 1.76−1.68 (m, 2H), 1.19−1.14 (d, 3H), 0.88−0.80 (m, 1H), 0.46−0.13 (m, 4H). *Boc-protecton of intermediate VI*: To a solution of secondary amine **VI** (43.0 g, 94.7 mmol, 1.0 equiv) in tetrahydrofuran/H_2O (1:1) (475 mL) at 0 °C were added Na_2CO_3 (15.1 g, 113.7 mmol, 1.5 equiv) and Boc_2O (24.8 g, 142.1 mmol, 1.2 equiv). The reaction mixture was then allowed to reach room temperature, whereupon it was stirred for 24 h, at which point the reaction was deemed complete by TLC (hexanes/EtOAc (1:1); R_f = 0.57 (UV)) and LCMS (method Grad_A4: retention time, 12.98 min). Tetrahydrofuran was evaporated under vacuum (15−30 mmHg) at 40−45 °C, and the residual aqueous phase was extracted with MTBE (3 × 100 mL). The combined organic extracts were washed with brine (1 × 100 mL), dried over $MgSO_4$, filtered, evaporated under vacuum (15−30 mmHg) at 40−45 °C, and dried under high vacuum (1−2 mmHg) at room temperature for 16−18 h to give the crude Boc-protected amino-ester **VII** as an orange oil (59.1 g, >100% crude yield). LCMS (method Grad_A4): retention time, 12.96 min; % purity (UV/ELSD/CLND), 86/100/94. [M + H]$^+$ = 555.37 (base peak at 441.32 corresponding to Boc-deprotected species). *Ester saponification of VII*: To a solution of the crude Boc-protected amino-ester **VII** (52.5 g, 94.7 mmol, 1.0 equiv) in tetrahydrofuran/H_2O (1:1) (475 mL) at room temperature was added LiOH·H_2O (19.9 g, 474 mmol, 5.0 equiv). The mixture was stirred 16−18 h at room temperature, whereupon the reaction was deemed complete by TLC (hexanes/AcOEt (1:1); R_f = 0 (UV)). The reaction mixture was acidified to pH 3.5 with citrate buffer (1M, pH 3.5), and tetrahydrofuran was then evaporated under vacuum (15−30 mmHg) at 40−45 °C. The residual aqueous phase was extracted with EtOAc (3 × 150 mL), and the combined organic extracts were washed with brine (1 × 100 mL), dried over $MgSO_4$, filtered, concentrated under vacuum (15−30 mmHg) at 40−45 °C, and dried under high vacuum (1−2 mmHg) at room temperature for 16−18 h to give carboxylic acid **VII** as a white gummy solid (47.3 g, 93% for 2 steps). LCMS (method Grad_A4): Retention time, 12.16 min; %purity (UV/ELSD/CLND), 96/100/95. [M + H]$^+$ = 541.37. ^{1}H NMR ($CDCl_3$) δ ppm 7.39−7.20 (m, 5H), 7.15−7.02 (m, 2H), 6.91 (d, 1H), 6.85−6.75 (m, 1H), 5.01 (s, 2H), 4.73−4.55 (m, 1H), 3.60−3.38 and 3.38−3.22 (m, 3H), 2.95 (br q, 2H) and 2.75−2.50 (m, 4H), 1.71−1.55 (m, 2H), 1.47−1.27 and 1.27−1.16 (m, 13H, with s at 1.35), 0.67−0.55 (m, 1H), 0.43−0.20 (m, 3H). HRMS obtained on a sample of Boc-deprotected **VII**; calculated for $C_{25}H_{32}N_2O_5$, 441.2390; found, 441.2373.

(R)-Benzyl 3-(4-Fluorophenyl)-2-((R)-2-(methylamino)-propanamido)propanoate (IX). Preparation of V as tosylate salt: To a suspension of H-(D)Phe(4F)-OH (55.6 g, 0.30 mol, 1.0 equiv) in toluene (1.2 L) was added *p*-toluenesulfonic acid (69.4 g, 0.37 mol, 1.2 equiv) and benzyl alcohol (157 mL, 1.52 mol, 5.0 equiv). The mixture was stirred at reflux 16−18 h in a Dean−Stark apparatus, whereupon it was allowed to reach room temperature thus producing a white precipitate. The precipitate was filtered, washed with MTBE (3 × 500 mL), and then dried under vacuum (1−2 mmHg) at room

temperature for 16−18 h to furnish the tosylate salt of H-(D)Phe(4F)-OH as a white solid (126 g, 93.1%). LCMS (method Grad_A4): retention time, 6.12 min; $[M + H]^+$ = 274.3. ^{1}H NMR (DMSO) δ ppm 8.40 (br s, 3H), 7.47−7.36 (d, 2H), 7.37−7.06 (m, 11H), 5.15 (s, 2H), 4.37 (t, 1H), 3.09−3.05 (m, 2H), 2.27 (s, 3H). ^{13}C NMR (DMSO) δ ppm 169.52 163.83, 160.62, 140.01, 138.56, 135.48, 132.16, 132.04, 131.33, 131.28, 129.09, 129.05, 128.84, 128.72, 127.09, 126.20, 116.18, 115.89, 67.83, 53.88, 35.83, 21.47. Melting point (uncorrected): 165−167 °C. *Preparation of V as free amine:* The tosylate salt obtained above (122 g) was added to an aqueous Na_2CO_3 solution (1M, 500 mL), and the resultant basic aqueous solution was extracted with EtOAc (4 × 500 mL). The combined organic extracts were washed with brine (1 × 250 mL), dried over $MgSO_4$, filtered, concentrated under vacuum (15−30 mmHg) at 40−45 °C, and then dried under high vacuum (1−2 mmHg) at room temperature to obtain the free amino-ester **V** as a white solid (74.4 g, 99%). ^{1}H NMR ($CDCl_3$) δ ppm 7.38−7.28 (m, 5H), 7.10−7.06 (m, 2H), 6.96−6.90 m, 2H, m), 5.13 (d, 2H), 3.76−3.71 (t, 1H), 3.07−2.83 (dq, 2H), 1.53 (s, 2H). *Dipeptide coupling to obtain **VIII**:* To a solution of free-based H-(D)Phe(4F)-OBn obtained above (74.4 g, 0.27 mol, 1.0 equiv) in anhydrous tetrahydrofuran/CH_2Cl_2 (1:1) (1120 mL) were added Boc-(D)NMeAla-OH (57.1 g, 0.28 mol, 1.03 equiv), 6-Cl-HOBt (46.2 g, 0.27 mol, 1.0 equiv), and iPr_2EtN (238 mL, 1.37 mol, 5.0 equiv). The mixture was cooled to 0 °C, and EDCI (57.6 g, 0.3 mol, 1.1 equiv) was added. The mixture was stirred 1 h at 4 °C, allowed to warm to room temperature, and stirred 16−18 h, whereupon the reaction was deemed complete by TLC (hexanes/EtOAc (4:6); R_f = 0.46 (UV/ninhydrin)). Thereupon, the volatiles were removed under vacuum (15−30 mmHg) at 40−45 °C. The residue thus obtained was dissolved in EtOAc (1000 mL) and washed successively with aqueous solution of citrate buffer (1M, pH 3.5) (2 × 500 mL), H_2O (1 × 500 mL), 0.1 M Na_2CO_3 (2 × 500 mL), and brine (1 × 500 mL). The organic extracts were dried over $MgSO_4$ (180 g), filtered, concentrated under vacuum (15−30 mmHg) at 40−45 °C then dried under high vacuum (1−2 mmHg) at room temperature for 16−18 h to give crude dipeptide **VIII** as yellow oil. (127 g, >100% crude yield). ^{1}H NMR ($CDCl_3$) δ ppm 7.40−7.25 (m, 5H), 7.00−6.83 (m, 4H), 5.26 (m, 2H), 4.85 (q, 1H), 4.68 (br s, 1H, br), 3.07 (ddd, 2H), 2.62 (s, 3H), 1.43 (s, 9H), 1.28 (d, 3H). ^{13}C NMR ($CDCl_3$) δ ppm 171.48, 163.77, 160.51, 135.21, 131.63, 130.94 (d), 128.87 (d), 115.61 (d), 80.96, 77.70, 77.47, 77.28, 76.85, 67.54, 53.28, 37.39, 29.82, 28.52, 15.51, 13.83. *Preparation of Boc-deprotected dipeptide **IX***: To a solution of crude Boc-protetced dipeptide **VIII** obtained in the previous step in dioxane (150 mL) was added a solution of 4 M HCl in dioxane (1360 mL, 20 equiv) and the resultant mixture stirred for 1 h at room temperature, whereupon Boc-deprotection was deemed complete by TLC (EtOAc/hexanes (3:2), R_f = 0 (UV/ninhydrin)). The mixture was then concentrated under high vacuum (1−2 mmHg) at 40−45 °C, and the residue was coevaporated (15−30 mmHg) at 40−45 °C with MTBE (2 × 500 mL) and then dried under high vacuum (1−2 mmHg) at room temperature. The crude dipeptide hydrochloride salt was obtained as a slightly yellow solid (96 g, 89.7%). The dipeptide hydrochloride salt **15** (96 g) was dissolved in hot EtOH (200 mL) and MTBE (900 mL) was slowly added to the hot solution, whereupon the mixture was allowed to reach room temperature and then stored at −20 °C for 16−18 h. The crystals thus obtained were filtered, washed with MTBE (2 × 200 mL), and then dried under vacuum (1−2 mmHg) at room temperature to furnish crystalline dipeptide hydrochloride **IX** (62 g, 64.5%). LCMS (method Grad_A4): retention time, 6.26 min; %purity (UV/ELSD/CLND), 99/100/98. $[M + H]^+$ = 359.20. Chiral HPLC: >99.9%. ^{1}H NMR (DMSO-d_6) δ ppm 9.31−9.28 (d, 1H), 7.38−7.26 (m, 7H), 7.09−7.04 (m, 2H), 5.10 (s, 2H), 4.65−4.57 (m, 1H), 3.76−3.69 (d, 1H), 3.15−3.08 and 2.99−2.91 (m, 2H), 2.22 (s, 3H), 1.31−1.28 (d, 3H). ^{13}C NMR (DMSO-d_6) δ ppm 171.33, 169.18, 137.63, 136.31, 129.92, 129.11, 128.95, 128.83, 128.63, 127.30, 67.00, 56.57, 54.38, 36.98, 31.11, 16.47. Melting point (uncorrected): 140−142 °C. HRMS calculated for $C_{20}H_{23}FN_2O_3$, 359.1771; found, 359.1750.

*(R)-2-((R)-2-((S)-2-(((R)-2-(2-(3-Aminopropyl)phenoxy)propyl)-amino)-2-cyclopropyl-N-methylacetamido)propanamido)-3-(4-fluorophenyl)propanoic acid (**XII**).* *Preparation of fully protected precursor **X***: To a solution of carboxylic acid **VII** (47.3 g, 87.6 mmol, 1.0 equiv) and dipeptide hydrochloride salt **IX** (36.2 g, 91.9 mmol, 1.05 equiv) in anhydrous tetrahydrofuran/CH_2Cl_2 (1:1) (438 mL) at 0 °C were added iPr_2EtN (92 mL, 526 mmol, 6.0 equiv) and HATU (34.9 g, 91.9 mmol, 1.05 equiv). The mixture was allowed to warm to room temperature and stirred 16−18 h, whereupon the reaction was deemed complete by TLC (EtOAc/hexanes (1:1); R_f = 0.48 (UV)). The mixture was concentrated under vacuum (15−30 mmHg) at 40−45 °C, and the residue was dissolved in EtOAc (250 mL). The organic phase was washed with an aqueous solution of citrate buffer (1M, pH 3.5) (3 × 150 mL), H_2O (1 × 150 mL), an aqueous solution of saturated $NaHCO_3$ (2 × 150 mL) and brine (1 × 150 mL). The organic phase was dried over $MgSO_4$, filtered, and concentrated under vacuum (15−30 mmHg) at 40−45 °C. Purification of the residue by silica gel flash chromatography (1 kg column) eluting with 10−50% gradient EtOAc/hexanes gave the protected alkylated tripeptide as a white gummy solid (70.0 g, 90%). LCMS (method Grad_A4): retention time, 15.06 min; %purity (UV/ELSD/CLND), 89/100/95. $[M + H]^+$ = 881.64. ^{1}H NMR ($CDCl_3$) δ ppm 7.10−6.50 (m, 13H), 4.90−4.75 (m, 2H), 4.70 (s, 2H), 4.53−4.18 (m, 2H), 4.02−3.85 (m, 1H), 3.40−2.97 (m, 2H), 2.88−2.60 (m, 3H), 2.60−2.40 (m, 1H), 2.40−2.10 (m, 4H) with 2.20 (s, 3H), 1.45−1.26 (m, 2H) 1.11 (s, 9H), 0.98−0.70 (m, 6H), 0.30−0 (br m, 3H). *Preparation of Benzyl and Cbz-deprotected precursor **XI***: To a suspension of Pd/C (10%) in EtOAc (150 mL) (13.8 g, 20% by weight) was added a solution of alkylated tripeptide **X** (69.0 g, 78.4 mmol, 1.0 equiv) in EtOAc (375 mL) and hydrogen was bubbled through the solution for 16−18 h, whereupon the reaction was deemed complete by TLC (EtOAc/hexanes (1:1); R_f = 0.22 (UV)). Excess hydrogen was purged by bubbling nitrogen through the reaction mixture, whereupon the mixture was filtered on a Celite pad and rinsed with EtOAc (3 × 125 mL). Volatiles were removed under vacuum (15−30 mmHg) at 40−45 °C to provide the Boc-protected amino-acid **XI** as white solid (51.4 g, 100%). LCMS (method Grad_A4): retention time 8.05 min; %purity (UV/ELSD/CLND), 97/100/98. $[M + H]^+$ = 657.57. ^{1}H NMR ($CDCl_3$) δ ppm 6.90−6.75 (m, 4H), 6.70−6.45 (m, 5H), 4.85−4.70 (br m, 1H), 4.55−4.35 (br m, 1H), 3.95−3.60 (m, 2H), 3.40−3.10 (br s, 1H), 3.10−2.85 (br s, 1H), 2.85−2.60 (dq, 2H), 2.50−2.30 (m, 3H), 2.30−2.15 (two s with overlapping m, 7H), 1.65−1.40 (br m, 2H), 1.33−0.70 (m, with s at 1.15 and d at 0.90, 15H), 0.28 to 0 (m, 5H). *Preparation of fully deprotected precursor **XII***: To amino acid **XI** (51.4 g, 78.4 mmol, 1.0 equiv) was added a solution of 3 M HCl in dioxane/H_2O (75:25) (525 mL, 1.57 mol, 20 equiv) and the mixture was stirred at room temperature 1.5 h, whereupon the solvent was evaporated under vacuum (1−2 mmHg) at 40−45 °C . The residue was subsequently azeotroped (15−30 mmHg) at 40−45 °C with toluene (3 × 150 mL) and then dried under vacuum (1−2 mmHg) at 40−45 °C to furnish the title linear precursor **XII** as an off-white solid (58.0 g, >100% crude yield). LCMS (method Grad_A4): retention time, 5.38 min; %purity (UV/ELSD/CLND), 94/100/97. $[M + H]^+$ = 557.43.

*(2R,5S,8R,11S)-5-Cyclopropyl-11-(4-fluorobenzyl)-2,7,8-trimethyl-4,5,7,8,10,11,13,14,15,16-decahydro-2H-benzo[q][1,4,7,10,13]-oxatetraazacyclooctadecine-6,9,12(3H)-trione (**2**).* To a solution of macrocyclic precursor **XII** (78.4 mmol, 1.0 equiv) in anhydrous tetrahydrofuran (1.57 L, 50 mM) were added DIPEA (68.0 mL, 392 mmol, 7.0 equiv) and DEPBT (25.8 g, 86.2 mmol, 1.1 equiv). The mixture was stirred at room temperature 16−18 h, whereupon the reaction was deemed complete by TLC (EtOAc/MeOH (9:1); R_f = 0.38 (UV)). Volatiles were removed under vacuum (15−30 mmHg) at 40−45 °C, and the residue thus obtained dissolved in a mixture of aqueous Na_2CO_3 (1 M, 500 mL) and EtOAc (250 mL). The separated basic aqueous phase was extracted with EtOAc (2 × 250 mL). The combined organic extracts were washed with brine (2 × 250 mL), dried over $MgSO_4$, filtered, and evaporated under vacuum (15−30 mmHg) at 40−45 °C. Purification of the residue by silica gel flash chromatography (550 g column) eluting with 100% EtOAc (2 L) and subsequently using gradient elution EtOAc/MeOH (99/1 to 98/2 to 95/5 to 90/10) afforded **2** as a pale-yellow solid (35.0 g, 83%,

combined for steps j and i, Scheme 1). The silica gel chromatographic purification can be replaced with the double crystallization procedures outlined below, which was applied in the case of scale-up. LCMS (method Grad_A4): retention time, 6.19 min; purity (UV/ELSD/CLND), 87/100/92. $[M + H]^+$ = 539.40 (cf. footnote 33 for the impurity profile). HRMS calculated for $C_{30}H_{39}FN_4O_4$, 538.2955; found, 538.2949. The free-base form of **2** (15.0 g, 27.9 mmol, 1.0 equiv) obtained above was dissolved in anhydrous EtOH (125 mL), to which was slowly added 1.25 M HCl in EtOH (33.0 mL, 41.8 mmol, 1.5 equiv), whereupon the mixture was stirred for 10 min at room temperature, then cooled to 0 °C and stirred for another 15 min. The mixture was then filtered cold, and the white precipitate was washed with cold anhydrous EtOH (2 × 75 mL). The solid was dried under vacuum (1−2 mmHg) at room temperature for 16−18 h to furnish **2**·HCl·EtOH as an amorphous white solid (13.1 g, 92%). LCMS (method Grad_A4): retention time, 6.18 min; purity (UV/ELSD/CLND), 99/100/100. $[M + H]^+$ = 539.35. To the thus obtained **2**·HCl·EtOH (13.9 g, 24.2 mmol) was added a mixture of EtOH/H_2O (92:8) (145 mL). The mixture was then heated to 75 °C to assist dissolution of the solid. The solution was then filtered hot, and the cloudy filtrate was once more heated at 75 °C to aid complete dissolution. The mixture was allowed to gradually reach room temperature over a 3 h period using an oil bath and was then stored at −20 °C for 16−18 h. The crystalline product thus obtained was collected by filtration, washed with cold anhydrous EtOH (1 × 75 mL) at room temperature, and subsequently dried under vacuum (1−2 mmHg) at room temperature for 16−18 h to provide **2**·HCl·EtOH as crystalline white solid (12.2 g, 88%). LC/MS (method Grad_A4): retention time, 6.18 min; purity (UV/ELSD/CLND), 100/100/100. $[M + H]^+$ = 539.35. The crystalline **2**·HCl·EtOH (11 g, 17.7 mmol) obtained in the previous step was dissolved in MEK−H_2O (11 mL: 44 mL) at 70−75 °C. The mixture was allowed to gradually reach room temperature over a 3 h period using an oil bath and then stored at 4 °C overnight. The thus obtained **2**·HCl·H_2O crystals were air-dried to constant weight (8.68 g, 83%). LCMS (method Grad_A4): retention time, 6.18 min; purity (UV/ELSD/CLND), 100/100/100. $[\alpha]^{25}_D$ = +61.8° ± 0.2 (*c* = 0.125, dimethyl formamide). ^{1}H NMR (CD_3OD): δ ppm 8.16 (d, 1H, *J* = 8.4 Hz), 7.13−7.32 (m, 4H), 6.89−7.07 (m, 4H), 4.86−4.91 (m, 1H), 4.38−4.47 (m, 2H), 4.28 (q, 1H, *J* = 7.3), 3.44−3.56 (m, 2H), 3.32−3.39 (m, 1H), 3.14 (s, 3H), 3.09−3.28 (m, 3H), 2.88 (ddd, 1H, *J* = 5.5, 10.7, 13.5 Hz), 2.64 (ddd, 1H, *J* = 5.5, 10.7, 13.5), 1.73−2.03 (m, 2H), 1.38 (d, 3H, *J* = 6.0 Hz), 1.33 (d, 3H, *J* = 7.5 Hz), 1.21−1.31 (m, 1H), 0.61−0.90 (m, 4H). ^{13}C (CD_3OD) δ ppm 173.4, 173.3, 170.0, 163.2 (d, *J* = 241.9), 155.3, 135.5 (d, *J* = 3.0), 133.0, 132.0 (d, *J* = 7.9 Hz), 131.8, 128.3, 123.0, 116.1 (d, *J* = 21.3 Hz), 114.1, 70.1, 62.8, 59.0, 57.1, 52.7, 41.8, 36.2, 34.5, 30.8, 29.8, 17.5, 14.6, 12.0, 5.0, 3.8. HRMS calculated for $C_{30}H_{39}FN_4O_4$, 538.2955; found, 538.2944. Anal. Calcd (found) for $C_{30}H_{42}ClFN_4O_5$: C, 60.75% (60.35%); H, 7.14% (7.08%); N, 9.45% (9.31%); Cl, 5.98% (5.94%).

■ ASSOCIATED CONTENT

Supporting Information

Complete set of data related to the X-ray crystallographic and solution NMR structural studies on compound **2** are provided. Experimental procedures for the synthesis of tethers and building blocks are detailed. Characterization data for building blocks (LC/MS, ^{1}H, ^{13}C NMR) and macrocycles (LCMS, HRMS, ^{1}H NMR, ^{13}C NMR) are furnished, including copies of HRMS spectra and LCMS chromatograms. This material is available free of charge via the Internet at http://pubs.acs.org.

■ AUTHOR INFORMATION

Corresponding Author

*Phone: +32-71-348-502. Fax: +32-71-348-519. E-mail: hhoveyda@euroscreen.com. Current address: Euroscreen SA, 47, rue Adrienne Bolland, 6041 Gosselies, Belgium.

■ ACKNOWLEDGMENTS

We thank Annie Doucet, Maude Gauthier, Annie Letendre, and Jacinthe Beausoleil for additional assistance with the analytical support of this work. We are indebted to Gaston Boulay and Dr. Daniel Fortin (Université de Sherbrooke) for providing the HRMS data and solving the X-ray crystal structures, respectively, and to Dr. Ken Rotondi (University of Massachusetts at Amherst) for initial help with setting up NMR structural studies in-house. Finally, we are grateful to Dr. Andy Vinter and Dr. Rob Scoffin at Cresset Biomolecular Discovery Ltd (UK) for discussions and calculations on the stereoelectronic *trans* lone pair effect and hydrophobic collapse in **2**.

■ DEDICATION

†This paper is dedicated to Professor Pierre Deslongchamps whose vision led to the founding of NéoKimia Inc. that in turn laid the basis for the work described herein.

■ ABBREVIATIONS USED

ADME, absorption, distribution, metabolism and excretion; API, advanced pharmaceutical ingredient; AUC, area under curve; CL, systemic clearance rate; 6Cl-HOBt, 6-chloro-1-hydroxybenzotriazole; C_{max}, maximal concentration; CYP, cytochrome P-450; DEPBT, 3-(diethoxyphosphoryl)-1,2,3-benzotriazin-4(3*H*)-one; EDCI, 1-ethyl-3-(3-dimethylaminopropyl)carbodiimide hydrochloride; %*F*, absolute oral availability; GE, gastric emptying; GH, growth hormone; GI, gastrointestinal; GPCR, G-protein coupled receptor; GRLN, human ghrelin receptor; H-Cpg-OH, (*S*)-amino-cyclopropyl-acetic acid; HATU, 1-[bis(dimethylamino)-methylene]-1*H*-1,2,3-triazolo-[4,5-*b*]pyridinium hexafluorophosphate 3-oxide; hERG, human ether-à-go-go related gene; HLM, human liver microsomes; HTS, high-throughput screening; LLE, ligand lipophilicity efficiency; IV, intravenous administration; MEK, methyl ethyl ketone; MOT-R, human motilin receptor; MTBE, *tert*-butylmethyl ether; NBS, *N*-bromosuccinimide; PD, pharmacodynamic; Pgp, P-glycoprotein; PK, pharmacokinetics; PO, per os (oral) administration; POI, postoperative ileus; RLM, rat liver microsomes; SAR, structure−activity relationship; $T_{1/2}$, elimination half-life; TLC, thin-layer chromatography; TsOH, *para*-toluene sulfonic acid; V_{dss}, steady-state volume of distribution

■ REFERENCES

(1) Clardy, J.; Walsh, C. Lessons from Natural Molecules. *Nature* **2004**, *432*, 829−837.

(2) Lipinski, C. A.; Lombardo, F.; Dominy, B. W.; Feeney, P. J. Experimental and computational approaches to estimate solubility and permeability in drug discovery and development settings. *Adv. Drug Delivery Rev.* **1997**, *23*, 3−25.

(3) (a) Trepanier, D. J.; Gallant, H.; Legatt, D. F.; Yatscoff, R. W. Rapamycin: Distribution, Pharmacokinetics and Therapeutic Range Investigations: An Update. *Clin. Biochem.* **1998**, *31*, 345−351. (b) Akhlagi, F.; Trull, A. K. Distribution of Cyclosporin in Organ Transplant Recipients. *Clin. Pharmacokinet.* **2002**, *41*, 615−637.

(4) Okumu, F. W.; Pauletti, G. M.; VanderVelde, D. G.; Siahaan, T. J.; Borchardt, R. T. Effect of restricted conformational flexibility on the permeation of model hepatocytes across Caco-2 cell monolayers. *Pharm. Res.* **1997**, *14*, 169−175.

(5) (a) Tonelli, A. F. The Effects of Isolated *N*-Methylated Residues on the Conformational Characteristics of Polypeptides. *Biopolymers* **1976**, *15*, 1615−1622. (b) Chatterjee, J.; Mierke, D.; Kessler, H. *N*-

Methylated Cyclic Pentaalanine Peptides as Template Structures. *J. Am. Chem. Soc.* **2006**, *128*, 15164−15172.

(6) Hoffmann, R. W. Conformation design of open-chain compounds. *Angew. Chem., Int. Ed.* **2000**, *39*, 2054−2070.

(7) Veber, D. F.; Johnson, S. R.; Cheng, H. Y.; Smith, B. R.; Ward, K. W.; Kopple, K. D. Molecular properties that influence the oral bioavailability of drug candidates. *J. Med. Chem.* **2002**, *45*, 2615−2623.

(8) Marsault, E.; Hoveyda, H. R.; Gagnon, R; Peterson, M. L.; Vézina, M.; Saint-Louis, C.; Landry, A.; Pinault, J.-F.; Ouellet, L.; Beauchemin, S.; Beaubien, S.; Mathieu, A.; Benakli, K.; Wang, Z.; Brassard, M.; Lonergan, D.; Bilodeau, F.; Ramaseshan, M.; Fortin, N.; Lan, R.; Li, S.; Galaud, F.; Plourde, V.; Champagne, M.; Doucet, A.; Bhérer, P.; Gauthier, M.; Olsen, G.; Villeneuve, G.; Bhat, S.; Foucher, L.; Fortin, D.; Peng, X.; Bernard, S.; Drouin, A.; Déziel, R.; Berthiaume, G.; Dory, Y. L.; Fraser, G. L.; Deslongchamps, P. Efficient parallel synthesis of macrocyclic peptidomimetics. *Biorg. Med. Chem. Lett.* **2008**, *18*, 4731−4735.

(9) For some recent reviews, see: (a) Driggers, E. M.; Hale, S. P.; Lee, J.; Terrett, N. K. The exploration of macrocycles for drug discovery—an underexploited structural class. *Nature Rev. Drug Discovery* **2008**, *7*, 608−624. (b) Marsault, E. M.; Peterson, M. L. Macrocycles are Great Cycles: Applications, Opportunities, and Challenges of Synthetic Macrocycles in Drug Discovery. *J. Med. Chem.* **2011**, *54*, 1961−2004.

(10) Marsault, E.; Hoveyda, H. R.; Peterson, M. L.; Saint-Louis, C.; Landry, A.; Vézina, M.; Ouellet, L.; Wang, Z.; Ramaseshan, M.; Beaubien, S.; Benakli, K.; Beauchemin, S.; Déziel, R.; Peeters, T.; Fraser, G. L. Discovery of new class of macrocyclic antagonists to the human motilin receptor. *J. Med. Chem.* **2006**, *49*, 7190−7197.

(11) Kojima, M.; Hosoda, H.; Date, Y.; Nakazato, M.; Matsuo, H.; Kangawa, K. Ghrelin is a growth- hormone-releasing acylated peptide from stomach. *Nature* **1999**, *402*, 656−660, Ghrelin amino acid sequence is as follows: GSS(*n*-octanoyl) FLSPEHQRVQQRKESKKPPAKLQPR. The octanoylated ghrelin peptide was used throughout the work herein..

(12) Davenport, A. P.; Bonner, T. I.; Foord, S. M.; Harmar, A. J.; Neubig, R. R.; Pin, J.-P.; Spedding, M.; Kojima, M.; Kangawa, K. International Union of Pharmacology. LVI. Ghrelin Receptor Nomenclature, Distribution, and Function. *Pharmacol. Rev.* **2005**, *57*, 541−546.

(13) Exemplified by this subclass are receptors such as GnRH, galanin, MCH, orexin, a number of chemokine receptors that are variously involved in obesity, eating and reproductive disorders, pain, inflammation and narcolepsy. See: Lavrador, K.; Murphy, B.; Saunders, J.; Struthers, S.; Wang, X.; Williams, J. A screening library for peptide activated G-protein coupled receptors. 1. The test set. *J. Med. Chem.* **2004**, *47*, 6864−6874.

(14) Howard, A. D.; Feighner, S. D.; Cully, D. F.; Arena, J. P.; Liberator, P. A.; Rosenblum, C. I.; Hamelin, M.; Hreniuk, D. L.; Palyha, O. C.; Andrerson, J.; Paress, P. S.; Diaz, C.; Chou, M.; Liu, K. K.; McKee, K. K.; Pong, S.-S.; Chaung, L.-Y.; Elbrecht, A.; Dashkevicz, M.; Heavens, R.; Rigby, M.; Sirinathsighji, D. J. S.; Dean, D. C.; Melillo, D. G.; Patchett, A. A.; Nargund, R.; Griffin, P. R.; DeMartino, J. A.; Gupta, S. K.; Schaeffer, J. M.; Smith, R. G.; Van der Ploeg, L. H. T. A receptor in pituitary and hypothalamus that functions in growth hormone release. *Science* **1996**, *273*, 974−977.

(15) Peeters, T. L. Ghrelin: A new player in the control of gastrointestinal functions. *Gut* **2006**, *54*, 1638−1649, and references therein.

(16) Levin, F.; Edholm, T.; Schmidt, P. T.; Grybäck, P.; Jacobsson, H; Degerblad, C.; Höybye, C.; Holst, J. J.; Rehfeld, J. F.; Hellström, P. M.; Näslund, E. Ghrelin stimulates gastric emptying and hunger in normal weight humans. *J. Clin. Endocrinol. Metab.* **2006**, *91*, 3279−3280.

(17) (a) Binn, M.; Albert, C.; Gougeon, A.; Maerki, H.; Coulie, B.; Lemoyne, M.; Rabasa Lhoret, R.; Tomasetto, C.; Poitras, P. Ghrelin gastrokinetic action in patients with neurogenic gastroparesis. *Peptides* **2006**, *27*, 1603−1606. (b) Tack, J.; Depoortere, I.; Bisschops, R.; Verbeke, K.; Janssens, J.; Peeters, T. Influence of ghrelin on gastric emptying and meal-related symptoms in idiopathic gastroparesis. *Aliment. Pharmacol. Ther.* **2005**, *22*, 847−853. (c) Murray, C. D.; Martin, N. M.; Patterson, M.; Taylor, S. A.; Ghatei, M. A.; Kamm, M. A.; Johnston, C.; Bloom, S. R.; Emmanuel, A. V. Ghrelin enhances gastric emptying in diabetic gastroparesis: a double blind, placebo controlled, crossover study. *Gut* **2005**, *54*, 1693−1698.

(18) (a) Fraser, G. L.; Venkova, K.; Hoveyda, H. R.; Thomas, H.; Greenwood-Van Meerveld, B. Effect of the ghrelin receptor agonist TZP-101 on colonic transit in a rat model of postoperative ileus. *Eur. J. Pharmacol.* **2009**, *604*, 132−137. (b) Lasseter, K. C.; Shaughnessy, L.; Cummings, D.; Pezzullo, J. C.; et al. Ghrelin agonist (TZP-101): Safety, pharmacokinetics and pharmacodynamic evaluation in healthy volunteers: A phase I, first-in-human study. *J. Clin. Pharm.* **2008**, *48*, 193−202. (c) Venkova, K.; Fraser, G.; Hoveyda, H. R.; Greenwood-Van Meerveld, B. Prokinetic effects of a new ghrelin receptor agonist TZP-101 in a rat model of postoperative ileus. *Dig. Dis. Sci.* **2007**, *52*, 2241−2248.

(19) (a) Popescu, I.; Fleshner, P. R.; Pezzullo, J. C.; Charlton, P. A.; Kosutic, G.; Senagore, A. J. The Ghrelin Agonist TZP-101 for Management of Postoperative Ileus After Partial Colectomy: A Randomized, Dose-Ranging, Placebo-Controlled Clinical Trial. *Dis. Colon Rectum* **2010**, *53*, 126−134. (b) Ejskjaer, N.; Dimcevski, G.; Wo, J.; Hellström, P. M; Gormsen, L. C.; Sarosiek, I.; Søfteland, E.; Nowak, T.; Pezzullo, J. C.; Shaughnessy, L.; Kosutic, G.; McCallum, R. Safety and efficacy of ghrelin agonist TZP-101 in relieving symptoms in patients with diabetic gastroparesis: a randomized, placebo-controlled study. *Neurogastroenterol. Motil.* **2010**, *22*, 1069−1078. (c) Wo, J. M.; Ejskjaer, N.; Hellström, P. M.; Malik, R. A.; Pezzullo, J. C.; Shaughnessy, L.; Charlton, P.; Kosutic, G.; McCallum, R. W. Randomised clinical trial: ghrelin agonist TZP-101 relieves gastroparesis associated with severe nausea and vomiting—randomised clinical study subset data. *Aliment. Pharmacol. Ther.* **2011**, *33*, 679−688.

(20) Fraser, G. L.; Hoveyda, H. R.; Tannenbaum, G. S. Pharmacological Demarcation of the Growth Hormone, Gut Motility and Feeding Effects of Ghrelin Using a Novel Ghrelin Receptor Agonist. *Endocrinology* **2008**, *149*, 6280−6288.

(21) For further comparison of the GH and GI effects of GRLN agonists in development for GI disorders, see: (a) Charoenthongtrakul, S.; Giuliana, D.; Longo, K. A.; Govek, E. K.; Nolan, A.; Gagne, S.; Morgan, K.; Hixon, J.; Flynn, N.; Murphy, B. J.; Hernández, A. S.; Li, J.; Tino, J. A.; Gordon, D. A.; DiStefano, P. S.; Geddes, B. J. Enhanced gastrointestinal motility with orally active ghrelin receptor agonists. *J. Pharmacol. Exp. Ther.* **2009**, *329*, 1178−1186. (b) Garcia, J. M.; Polvino, W. J. Pharmacodynamic hormonal effects of of anamorelin, a novel oral ghrelin mimetic and growth hormone secretagogue in human volunteers. *Growth Horm. IGF Res.* **2009**, *19*, 267−273. (c) Datta, R.; Soulard, C.; Teillot, M.; Touvay, C.; Halem H.; Dong, J. Z.; Culler, M. D. RM-131: a potent gastroprokinetic agent. *Gastroenterology* **2011**, *140*(5), *Suppl 1*, S-25. (d) Pietra, C.; Friend, J.; Greenwoord-van Meerveld, B. Preclinical pharmacological profile of ipamorelin a novel gastroprokinetic for intestinal dysmotility. *Gastroenterology* **2011**, *140*(5), *Suppl 1*, S-285.

(22) For some recent reviews, see: (a) Moulin, A.; Ryan, J.; Martinez, J.; Fehrentz, J.-M. Recent Developments in Ghrelin Receptor Ligands. *ChemMedChem* **2007**, *2*, 1242−1257. (b) Costantino, L.; Barlocca, D. Ghrelin receptor modulators and their therapeutic potential. *Fut. Med. Chem.* **2009**, *1*, 157−177.

(23) Holst, B.; Brandt, E.; Bach, A.; Heding, A.; Schwartz, T. W. Nonpeptide and peptide growth hormone secretagogues act both as ghrelin receptor agonist and as positive or negative allosteric modulators of ghrelin signaling. *Mol. Endocrinol.* **2005**, *19*, 2400−2411.

(24) The ligand activation domain of GRLN is highly conserved across species and is most closely homologous to the MOT-R, which is 52% identical to GRLN with 86% identity in the transmembrane domains. See: Coulie, B.; Matsuura, B.; Dong, M.; Hadac, E. M.; Pinon, D. I.; Feighner, S. D.; Howard, A. D.; Miller, L. J. Identification of peptide ligand-binding domains within the human motilin receptor

using photoaffinity labeling. *J. Biol. Chem.* **2001**, *276*, 35518−35522, and references therein.

(25) A solution phase variant of method A was also developed and employed for the synthesis of analogues **49**−**50**. (cf. footnote 31 and Scheme III in the Supporting Information).

(26) During method A syntheses, loss of resin loading was observed mainly at the AA_1 coupling (likely due to diketopiperazine formation) and during the Fukuyama−Mitsunobu steps. However, this was not prohibitive to obtaining the desired macrocycles in sufficient quantity, whether in small scale library syntheses, or in 0.1−0.5 g scale-ups using the method A procedure.

(27) Humphrey, J. M.; Chamberlin, A. R. Chemical synthesis of natural product peptides: coupling methods for the incorporation of noncoded amino acids into peptides. *Chem. Rev.* **1997**, *97*, 2243−2266.

(28) Carpino, L. A.; Imazumi, H.; El-Faham, A.; Ferrer, F. J.; Zhang, C.; Lee, Y.; Foxman, B. M.; Henklein, P.; Hanay, C.; Mügge, C.; Wenschuh, H.; Klose, J.; Beyermann, M.; Bienert, M. The uronium/guanidinium peptide coupling reagents: finally the true uronium salts. *Angew. Chem., Int. Ed.* **2002**, *41*, 441−445.

(29) The HPLC purity of all final products was determined using three detectors (UV, ELSD, and CLND) to ascertain a purity level of ≥95%. (CLND stands for "**c**hemi**l**uminescence **n**itrogen **d**etector" and ELSD for "**e**vaporative **l**ight-**s**cattering **d**etector"). CLND was also used for HTS compound quantification; cf.: Taylor, E. W.; Qian, M. G.; Dellinger, G. D. Simultaneous On-Line Characterization of Small Organic Molecules Derived from Combinatorial Libraries for Identity, Quantity, and Purity by Reversed-Phase HPLC with Chemiluminescent Nitrogen, UV, and Mass Spectrometric Detection. *Anal. Chem.* **1998**, *70*, 3339−3347.

(30) In the scale-up procedure, Boc-protection of the secondary amine (step f) to form **VII** was omitted; thus, unprotected amine was directly used in coupling with fragment **IX** and in the subsequent steps. (Cf. footnote 33 for further clarification).

(31) In the early attempts towards a macrocycle solution synthesis, the AA_1-tether fragment (step d) was prepared through a Fukuyama−Mitsunobu strategy akin to that in solid-phase method A. As overalkylation in H-Cpg-OMe proved to be a limited side-reaction, the more efficient direct alkylation strategy was selected as the methodology of choice.

(32) Li, H.; Jiang, X.; Ye, Y.; Fan, C.; Romoff, T.; Goodman, M. 3-(Diethoxyphosphoryloxy)-1,2,3-benzotriazin-4(3*H*)-one (DEPBT): a new coupling agent with remarkable resistance to racemization. *Org. Lett.* **1999**, *1*, 91−94.

(33) Two principle process impurities were identified by LCMS as shown below. Impurity **A** originated at the acidolytic Boc-deprotection step. To remedy this, the Boc-protection strategy was eliminated (steps f, j in Scheme 1) and successfully implemented in the API scale-up campaign. Impurity **B** is the expanded macrocyclic dimer of **2** that arose at the macrocyclization stage (step k) proportional to the reaction mixture concentration.

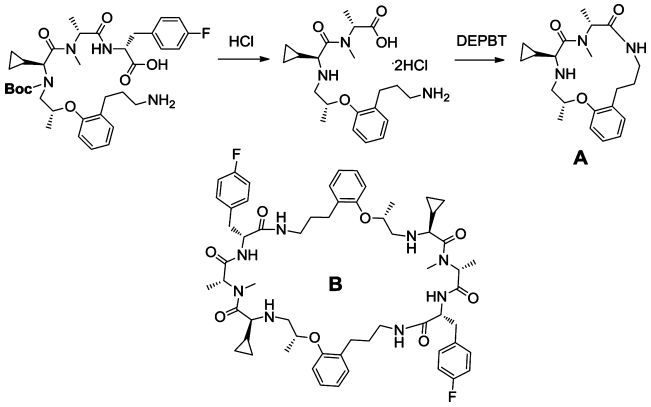

(34) (a) See p 333 in reference 50a in particular; (b) This observation was further elaborated by Richardson and Richardson wherein the conformational consequences on backbone and side-chain are discussed when Val/Ile vs Leu and Met/Thr vs Ser are incorporated into peptide sequences. See: Richardson, J. S.; Richardson, D. C. Principles and Patterns of Protein Conformation. In *Prediction of Protein Structure and the Principles of Protein Conformation*; Fasman, G. D., Ed.; Plenum Press: New York and London, 1989; pp 59−62.

(35) van de Waterbeemd, H.; Smith, D. A.; Beaumont, K.; Walker, D. K. Property-Based Design: Optimization of Drug Absorption and Pharmacokinetics. *J. Med. Chem.* **2001**, *44*, 1313−1333, and reference 201 therein.

(36) (a) Similarly in an elegant study by De Grado et al., the most potent of their 18-membered cyclic peptides contained both an *N*-methyl and a D-amino acid (D-Abu-NMe-Arg fragment) that induced a β-turn, which was shown by NMR studies to be key to conformational rigidity. See: Bach, A. C. II; Eyermann, C. J.; Gross, J. D.; Bower, M. J.; Harlow, R. L.; Weber, P. C.; DeGrado, W. F. Structural studies of a family of high affinity ligands for GPIIa/IIIa. *J. Am. Chem. Soc.* **1994**, *116*, 3207−3219. (b) Steric interactions among side-chain residues are recognized as the driving force for a β-turn (cf. ref 51). Searle et al. (ref 57) noted that the population of β-space (so-called P_β) in a tripeptide varies with the highest P_β values observed when central amino acids are flanked by β-branched aliphatic or aromatic residues; this is the case in the advanced leads herein (AA_1 = Cpg and AA_3 = D-Phe derivatives).

(37) LLE = pK_i − clogP, i.e. "the quantity of potency per unit of lipophilicity" as stated in the reference below. Rule-of-five concerns demand LLE ≥ 5.5 for optimal clinical targets. Note that given the $pK_a \approx 7$ in the foregoing macrocycles (cf. footnote 61), the LLE values cited herein (using clogP) are *only intended to depict the relative LLE trends*. See: Edwards, M. P.; Price, D. A. Role of Physicochemical Properties and Ligand Lipophilicity Efficiency in Addressing Drug Safety Risks. *Annu. Rep. Med. Chem.* **2010**, *45*, 381−391.

(38) Thus, **2**: AA_3 = D-Phe(4-F), LLE = 1.5 > **30**: AA_3 = D-Phe, LLE = 1.3 > **16**: AA_3 = D-Phe(4-Cl), LLE = 1.0. (cf. footnote 37).

(39) Hruby, V. J.; Li, G.; Haskell-Luevano, C.; Shanderovich, M. Deisgn of peptides, proteins and peptidomimetics in chi space. *Biopolymers* **1997**, *43*, 219−266, and references therein.

(40) Thus, **44**: phenyl tether, LLE = −0.35 vs **17**: phenoxy tether, LLE = 1.46 (cf. footnote 37).

(41) The MOT-R K_i values are as follows: **17**, K_i = 10.7 μM; **41**, K_i = 4.6 μM. For analogue **41**, the most potent of the two olefin stereoisomers, i.e. GRLN K_i = 160 nM was tested against MOT-R.

(42) (a) Vieth, M.; Siegel, M. G.; Higgs, R. E.; Watson, I. A.; Robertson, D. H.; Savin, K. A.; Durst, G. L.; Hipskind, P. A. Characteristic Physical Properties and Structural Fragments of Marketed Oral Drugs. *J. Med. Chem.* **2004**, *47*, 224−232. (b) Wenlock, M. C.; Austin, R. P.; Barton, P.; Davis, A. M.; Leeson, P. D. A Comparison of Physicochemical Property Profiles of Development and Marketed Oral Drugs. *J. Med. Chem.* **2003**, *46*, 1250−1256.

(43) Both experimental data and MO calculations show that in a cyclopropyl ring external orbitals ring have ∼33% *s* character (∼sp^2 orbitals), while the internal orbitals (through which C−C bonds are formed) have ∼17% *s* character (∼sp^5 orbitals). Thus, the "bent bonds" in a cyclopropyl ring directs electron density *away from the ring* as opposed to the case in typical C_{sp3}−C_{sp3} bonds where electron density is symmetrically distributed along the internuclear bond axis. The potential impact of the enhanced electron-donating effect of cyclopropyl ring in modulating PK properties in **2** is elaborated further below in the text. For some relevant references, see: (a) Cremer, D.; Kraka, E. Theoretical determination of molecular structure and conformation. 15. Three-membered rings: bent bonds, ring strain, and surface delocalization. *J. Am. Chem. Soc.* **1985**, *107*, 3800−3810. and 3811−3819. (b) de Meijere, A. Bonding properties of cyclopropane and their chemical consequences. *Angew. Chem. Int. Ed* **1979**, *18*, 809−826. (c) Wiberg, K. B. Bent bonds in organic compounds. *Acc. Chem. Res.* **1996**, *29*, 229−234.

(44) The long $T_{1/2}$ of 74 min for analogue **38** mirrors the large V_{dss} term that is in turn likely a reflection of the lipophilicity of the cyclohexyl side-chain. Extremely poor aqueous solubility in **38** is consistent with the said observations.

(45) Study conducted at Covance Laboratories Inc., Madison, WI. Compound was dosed in 5% dextrose in water (with sodium acetate buffer). Biliary excretion is common in both cyclic peptides and peptidomimetics; e.g., see: (a) Veber, D. F.; Saperstein, R.; Nutt, R. F.; Freidinger, R. M; Brady, S. F.; Curley, P.; Perlow, D. S.; Paleveda, W. J.; Colton, C. D.; Zacchei, A. G.; Tocco, D. J.; Hoff, D. A.; Vandlen, R. L.; Gerich, J. E.; Hall, L.; Mandarino, L.; Cordes, E. H.; Anderson, P. S.; Hirschmann, R. A Super Active Cyclic Hexapeptide Analog of Somatostatin. *Life Sci.* **1984**, *34*, 1371−1378. (b) Llinàs-Burnet, M.; Bailey, M. D.; Bolger, G.; Brochu, C.; Faucher, A.-M.; Ferland, J. M.; Garneau, M.; Ghiro, E.; Gorys, V.; Grand-Maître, C.; Halmos, T.; Lapeyre-Paquette, N.; Liard, F.; Poirier, M.; Rhéaume, M.; Tsantrizos, Y. S.; Lamarre, D. Structure−Activity Study on a Novel Series of Macrocyclic Inhibitors of the Hepatitis C Virus NS3 Protease Leading to the Discovery of BILN 2061. *J. Med. Chem.* **2004**, *47*, 1605−1608.

(46) Equilibrium protein binding results were obtained by ultracentrifugation method. Rat and human plasma protein binding were 87 ± 3% and 98.4 ± 0.6%, respectively, at 5 μg/mL compound concentration. Human PK data for compound **2** (ref 18b) revealed a low CL (5 mL/h/kg, at 20 μg/kg dose) and a long $T_{1/2}$ of 12.6 h. The low volume of distribution in man (V_{dss}= 0.08 L/kg) versus a much larger value in rats (V_d = 1.7 L/kg, cf. Table 4) is consistent with the protein binding trends.

(47) The difference in dose used in acquisition of rat vs monkey PK data in Tables 5−6 is noted. That this was not a reason for the species PK differentiation observed in **2** vs **51** was confirmed by verification of the rat PK results using the lower dose applied in monkey studies. Thus, in rats dosed IV at 0.5 mg/kg and PO at 1.5 mg/kg, the following PK parameters were determined: **2**, CL = 23 mL/min/kg and %F = 16 and for **51**, CL = 28 mL/min/kg and %F = 36; these are approximately the same as the rat PK data reported in Table 5 (at higher administered doses).

(48) Ghrelin peptide does not contain a Tyr residue (cf. footnote 12); thus, His-9 was iodinated in the preparation of the radioligand; see: Katugampola, S. D.; Pallikaros, Z.; Davenport, A. P. [^{125}I-His(9)]-ghrelin, a novel radioligand for localizing GHS orphan receptor in human and rat tissue: up-regulation of receptors with atherosclerosis. *Br. J. Pharmacol.* **2001**, *134*, 143−149.

(49) The aequorin assay was conducted at Euroscreen SA (Belgium). GRLN is stably expressed in CHO cell lines co-expressing mitochondrially-targeted apoaequorin. Aequorin is a photoprotein isolated form the jellyfish *Aequorea victoria* that upon Ca^{2+} binding oxidizes coelenterazine into coelenteramide with concomitant release of CO_2 and emission of light. The affinity of aequorin to Ca^{2+} is in the low μM range and its activity is proportional to the Ca^{2+} concentration in the physiological range (50 nM to 50 μM). Upon receptor activation, light is emitted for 20−30 s; thus, the bioluminescence readout provides a reliable tool to measure Ca^{2+} concentration, a secondary messenger in the PLCβ/IP_3/PKC signal transduction pathway of G_q-coupled GPCR receptors such as GRLN; see: Brini, M; Marsault, R.; Bastianutto, C.; Alvarez, A.; Pozzan, T.; Rizzuto, R. Transfected Aequorin in the Measurement of Cytosolic Ca^{2+} Concentration. *J. Biol. Chem.* **1995**, *270*, 9896−9903.

(50) Torsion angle data are detailed in the Supporting Information. Torsion angles (ϕ, ψ, ω) define peptide conformation through angle definitions as follows: ϕ, is the angle formed by C(O)−N−Cα-C(O), ψ, by N−Cα−C(O)−N, and ω, or the "amide torsion angle", by Cα−C(O)−N−Cα (thus ω = 180° for *trans* and 0° for *cis* amide bonds). See: (a) Ramachandran, G. N.; Sasisekharan, V. Conformation of polypeptides and proteins. *Adv. Protein Chem.* **1968**, *23*, 283−437. (b) Chou, P. Y.; Fasman, G. D. Prediction of the secondary structure of proteins from their amino acid sequence. *Adv. Enzymol.* **1978**, *47*, 45−148.

(51) Rose, G. D.; Gierasch, L. M.; Smith, J. A. Turns in Peptides and Proteins. *Adv. Protein Chem.* **1985**, *37*, 1−109.

(52) Turns structures have been further classified into "open" or "closed" categories by Rose et al. (ref 51). Thus, a closed turn contains a transannular H-bond between the C═O at the *i*th residue and the N−H at the (*i* + 3) residue, but no such H-bond exists in an open turn. Consequently, the NH_{i+3}−O_i distance is a determinant of the open or closed turn categorization. In **2**·HCl·H_2O and **2**·HCl·2H_2O open turns were observed, because the NH_{i+3}−O_i distances (3.34−3.42 Å) were significantly longer than the sum of the van der Waals radii for oxygen and hydrogen (2.72 Å). The other solvates of **2** (cf. Figure 4) contained closed turns. (See Supporting Information for details).

(53) Ruiz-Gomez, G.; Tyndall, J. D. A.; Pfeiffer, B.; Abbenante, G.; Fairlie, D. P. Over one hundred peptide-activated G protein coupled receptors recognize ligands with turn structure. *Chem. Rev.* **2010**, *110*, PR1−PR41.

(54) Bondi, R. A. van der Waals Volumes and Radii. *J. Phys. Chem.* **1964**, *68*, 441−451, Either Pauling's or Allinger's van der Waals radii can be used in the foregoing context with the same outcome.

(55) This observation holds in several solvents used: CD_3OD, CD_3CN, DMSO-d_6 and D_2O.

(56) Given a lack of consensus in nonpeptide structures for the parametrized Karplus equation, as evinced through the wide range of values cited in the literature, we limited this analysis solely to the (*i* + 2) residue, i.e. the AA_3 amide (cf. Figure 4b).

(57) It has been recognized that unstructured peptides are prone to conformational averaging and show an average coupling constant of ∼7 Hz, with larger coupling constants indicative of either α- or β-conformational; e.g., see: Griffiths-Jones, S. R.; Sharman, G. J.; Maynard, A. J.; Searle, M. S. Modulation of intrinsic ϕ, ψ propensities of amino acids by neighbouring residues in the coil regions of protein structures: NMR analysis and dissection of a β-hairpin peptide. *J. Mol. Biol.* **1998**, *284*, 1597−1609.

(58) The following coupling constants were measured for the (*i* + 2) and (*i* + 3) amides, i.e. the AA_3 and tether amides (cf. Fig 4b), respectively: CD_3OD (8.5 ± 0.5 Hz, 4.8 ± 0.4 Hz); CD_3CN (9.2 ± 0.2 Hz, 4.7 ± 0.2 Hz); DMSO)-d_6 (9.3 ± 0.1 Hz, 4.9 ± 0.3 Hz), H_2O−D_2O (8, 4.9). An ensemble of interconverting conformations would have led to average coupling constants of similar values in the 5−7 Hz range; e.g., see: Bogusky, M. J.; Naylor, A. M.; Pitzenberger, S. M.; Nutt, R. F.; Brady, S. F.; et al. NMR and molecular modeling characterization of RGD containing peptides. *Int. J. Peptide Protein Res.* **1992**, *39*, 63−76.

(59) Llinas, M.; Klein, M. P. Solution conformation of the ferrichromes. VI. Charge relay at the peptide bond. Proton magnetic resonance study of solvation effects on the amide electron density distribution. *J. Am. Chem. Soc.* **1975**, *97*, 4731−4737. (See Supporting Information for details on temperature-dependence NMR amide shifts in **2**.)

(60) Compare the following Hammett σ_p and Hansch π values: *n*-Pr (1.55, −0.13), cyclopropyl (1.14, −0.21) and cyclohexyl (2.51, −0.22). Values from: Kubinyi, H. In *Burger's Medicinal Chemistry and Drug Discovery*, 5th ed.; Wolff, M. E.; John Wiley & Sons: New York, 1995; Vol. *1*, Chapter 14, pp 497−571.

(61) The pK_a values were determined by potentiometry in the pH 3.5−10.5 range at *p*ION Inc., Woburn, MA. Reported errors are three times the standard deviation based on nonlinear regression analysis. These values are consistent with the reported pK_a for secondary amines in di- or tripeptides (pK_a ≈ 7−8). See: *Chemistry of Amino Acids*; Greenstein, J. P.; Winitz, M., Eds. John Wiley & Sons: New York, ; Vol. *1*, pp 488−491.

(62) In the R_2 = (*S*)-Me tether, the methyl moiety does *not* possess the appropriate topological orientation to enforce the shielding effect; it leaves one face of the macrocycle exposed for water attack that can in turn result in disruption of the intramolecular H-bond.

(63) Barreiro, E. J.; Kümmerle, A. E.; Fraga, C. A. M. The Methylation Effect in Medicinal Chemistry. *Chem. Rev.* **2011**, *111*, 5215−5246.